COMMUN. MATH. SCI.
Vol. 20, No. 7, pp. 1839–1873

A SECOND-ORDER WELL-BALANCED LAGRANGE-PROJECTION NUMERICAL SCHEME FOR SHALLOW WATER EXNER EQUATIONS IN 1D AND 2D*

CHRISTOPHE CHALONS† AND ALESSIA DEL GROSSO‡

Abstract. The present work is devoted to the numerical approximation of the shallow water Exner system in both one and two dimensions, where the Exner equation expresses the evolution in time of the bed sediment. Both the Grass and the Meyer-Peter & Müller formulas are taken into account to model the solid transport discharge contributions. The numerical scheme is based on the Lagrange-projection formalism which consists in splitting the mathematical model into the acoustic and transport systems. This work is considered as a first step to understand how to include the Exner equation in this framework and, for this reason, the Exner equation is taken into account only at the transport level; both a decoupled and weakly coupled formulations are proposed. New strategies to include the Exner equation at the acoustic level or in both steps will be treated in the next work. The methods are designed in such a way to satisfy the well-balanced property as well. Details to reach the second-order of accuracy are given; numerical results are shown to validate the numerical schemes.

Keywords. Lagrange-projection decomposition; Shallow water equations; Exner equation; Non-conservative hyperbolic systems; Second order of accuracy; Well-balanced property.

AMS subject classifications. 65N08; 76M12; 35L60.

1. Introduction and governing equations

This work deals with the design and implementation of a second-order well-balanced Lagrange-projection scheme applied to the 1D and 2D shallow water system with bed sediment non-constant in time. Lagrange-Projection (LP) approach consists in splitting the acoustic and transport waves of the model, leading to the possibility of approximating the two resulting systems with different approaches. This reveals itself to be useful, for instance, in subsonic regimes, where the acoustic waves are the reason for the restrictive CFL condition one has to employ in order to have a stable numerical scheme. Indeed, the Lagrange-projection decomposition makes possible to implicitly approximate only the acoustic system and, thus, to circumnavigate the problem of restrictive time-steps.

Nowadays, the Lagrange-projection approach has been studied in order to satisfy different properties and has been applied to several models. Giving a few examples, we refer, for instance, to the work [17], where all-regime first-order explicit and semi-implicit Lagrange-projection schemes have been applied to the gas dynamics model in several dimensions, or to [18], where the scheme was extended to the 2D two-phase flows model. Another possible reference is [9] with the numerical approximation of low Mach number flows of the barotropic Euler equations where the asymptotic-preserving property is satisfied as well. On the other hand, when it comes to the modeling of the shallow water system in the Lagrange-projection formalism, we can refer to [19] for an implicit well-balanced first-order scheme, to [14] for a fully well-balanced first-order explicit method, and finally to [39] for high-order fully well-balanced schemes. Last but

*Received: March 12, 2021; Accepted (in revised form): January 27, 2022. Communicated by François Bouchut.

†Université Paris-Saclay, Université de Versailles Saint-Quentin-en-Yvelines (UVSQ), CNRS, Laboratoire de Mathématiques de Versailles, 78000, Versailles, France (christophe.chalons@uvsq.fr).

‡Université Paris-Saclay, UVSQ, CNRS, Laboratoire de Mathématiques de Versailles, 78000, Versailles, France (alessia.del-grosso@ens.uvsq.fr).

not least, and without being exhaustive, we refer, for instance, to [8,11,23,24,32,33] for other interesting studies in this framework.

While details for the Lagrange-projection splitting are given in the following section, let us present now the mathematical model we are interested in. It is composed of two different ones, the hydrodynamic and the morphodynamic model. The former is simply given by the well-known shallow water system, which is derived from the Navier-Stokes system under the hypothesis that the vertical scale is much smaller than the horizontal dimension. As such, it is composed of the continuity and momentum equations, which are expressed as in the following

$$\begin{cases} \partial_t h + \partial_x(hu) = 0 \\ \partial_t(hu) + \partial_x(hu^2 + \frac{gh^2}{2}) = -gh\partial_x z \end{cases} \tag{1.1}$$

where $h(x,t) > 0$ is the water depth, $u(x,t)$ the averaged velocity and $z(x,t)$ the bed level. In particular, $H = h + z$ is the free surface elevation. Finally, g is the gravitational acceleration, $t > 0$ represents the time and x the axial coordinate. Let us briefly recall that this system is strictly hyperbolic with real eigenvalues given by $u \pm c$ with sound speed $c = \sqrt{gh}$.

Then, we aim to simulate the interaction between the sediments and the flow, thus we consider the topography z not constant in time and we make use of the so-called Exner equation, which reads

$$\partial_t z + \zeta \partial_x q_b = 0. \tag{1.2}$$

Here $q_b = q_b(h,u)$ is the solid transport discharge, $\zeta = \frac{1}{1-\rho_0}$ and ρ_0 is the porosity of the sediment layer. The coupling of (1.1) and (1.2) leads to the final system,

$$\begin{cases} \partial_t h + \partial_x(hu) = 0 \\ \partial_t(hu) + \partial_x(hu^2 + \frac{gh^2}{2}) + gh\partial_x z = 0 \\ \partial_t z + \zeta \partial_x q_b = 0, \end{cases} \tag{1.3}$$

which in compact form reads

$$\partial_t \mathbf{Q} + \partial_x \mathbf{F}(\mathbf{Q}) + \mathbf{A}(\mathbf{Q})\partial_x \mathbf{Q} = \mathbf{O}$$

where

$$\mathbf{Q} = \begin{pmatrix} h \\ hu \\ z \end{pmatrix}, \quad \mathbf{F}(\mathbf{Q}) = \begin{pmatrix} hu \\ hu^2 + p \\ \zeta q_b \end{pmatrix}, \quad \mathbf{A}(\mathbf{Q}) = \begin{pmatrix} 0 & 0 & 0 \\ 0 & 0 & gh \\ 0 & 0 & 0 \end{pmatrix}$$

with the pressure term $p = \frac{gh^2}{2}$. For details about shallow-water equations with and without non-constant in time bed sediment, we refer, for instance, to [3,6,10,12] and [1,7,14,38,44].

It is known that there exist different formulations to express the solid transport discharge q_b, depending on the characteristics of the sediment and the flow, for instance the Froude number, the slope of the bottom or the grain size. One of the easiest and most frequently used formulation is the well-known Grass model, which expresses the instantaneous sediment transport as a power law of the averaged velocity u, namely

$$q_b = A_g u|u|^{m_g - 1}, \quad 1 \le m_g \le 4, \tag{1.4}$$

refer to [5, 40]. This deterministic Grass formulation is suitable to model non-cohesive granular sediment. Here $A_g \in [0,1]$ is usually measured experimentally and expresses the type of interaction between the fluid and the sediment, whose strength increases as A_g approaches to 1. In particular, the value of the constant A_g is related to factors as the grain size and the kinematic viscosity. Finally, we set $m_g = 3$.

In this work we will mainly take into account the Grass model, only in one of the numerical tests the Meyer-Peter & Müller formula is also considered, see directly Section 5.3 or refer to [40] for details about other possible formulations for q_b. Moreover, it is important to stress that, depending on the formulation used for q_b, system (1.3) may or may not be hyperbolic. In particular, in [12] it has been confirmed that considering the Grass formula leads to a strictly hyperbolic system with all real eigenvalues. Indeed, defining the quantities

$$a_1 = -2u, \quad a_2 = u^2 - c^2(1 + \zeta \partial_{hu} q_b) \quad \text{and} \quad a_3 = -\zeta c^2 \partial_h q_b,$$

one can easily see that the eigenvalues are given by the solution of the following equation

$$\lambda^3 + a_1 \lambda^2 + a_2 \lambda + a_3 = 0.$$

Hence, the three eigenvalues read

$$\lambda_k = 2\sqrt{-p}\cos\Big(\frac{\theta + 2k\pi}{3}\Big) - \frac{a_1}{3} \quad \text{with} \quad k = 0,1,2 \tag{1.5}$$

where

$$p = \frac{3a_2 - a_1^2}{9}, \quad r = \frac{9a_1a_2 - 27a_3 + 2a_1^3}{54} \quad \text{and} \quad \theta = \arccos\Big(\frac{r}{\sqrt{-p^3}}\Big).$$

We remark that, in order to have real eigenvalues, we need $p^3 + r^2 \leq 0$, which can be proved in the case of the Grass model.

As mentioned at the very beginning of this work, we are also looking for a well-balanced numerical scheme, namely able to preserve the smooth stationary solutions of the system, that is to say the steady states which satisfy the ordinary differential equations

$$\partial_x(hu) = 0, \quad \partial_x\Big(hu^2 + \frac{gh^2}{2}\Big) + gh\partial_x z = 0 \quad \text{and} \quad \partial_x q_b = 0,$$

and obey

$$q = hu = \text{constant} = q_0, \quad \frac{q_0^2}{2h^2} + g(h+z) = \text{constant} \quad \text{and} \quad q_b = \text{constant}.$$

Note that if we use the Grass formula for q_b, then the only nontrivial stationary solutions are given by

$$u = 0 \quad \text{and} \quad h + z = \text{constant}, \tag{1.6}$$

which is called "lake at rest" equilibrium. For well-balanced schemes for the shallow-water equations, see for instance [1, 7, 36, 37], while for well-balanced methods in the Lagrange-projection formalism we refer to [14, 19, 39]. As far as the evolution in time of the bed sediment is considered as well, for general well-balanced schemes we refer, for instance, to [5, 31].

Outline of the paper. For the sake of clarity, let us briefly give the paper structure. In the next Section 2, the Lagrange-projection splitting is presented considering both Eulerian and Lagrangian variables. A brief summary of the approximate Riemann solver for the acoustic system is outlined as well. In Section 3, both first and second-order numerical schemes are described, distinguishing between acoustic and transport steps. Then, the two-dimensional extension of the mathematical model and the numerical method are illustrated in Section 4. Finally, Section 5 is exploited to present the numerical results and validate our numerical schemes. Concluding, final remarks are drawn in Section 6.

2. Operator splitting and Lagrangian coordinates

In this section we briefly explain the decomposition which entails the splitting of system (1.3) into two different ones, the so-called acoustic and transport systems. The former takes into account the acoustic effects of the model and the source term related to the topography, while the latter the transport phenomena. We will see further that this splitting can be interpreted as a Lagrange-projection one, as we first formulate the shallow-water system in Lagrangian coordinates (acoustic step) and then we project the solution into Eulerian coordinates (transport step). For more details about this decomposition, the reader can refer to [14, 19, 39].

Considering first only the shallow water system, it can be reformulated as

$$\begin{cases} \partial_t h + h\partial_x u + u\partial_x h = 0 \\ \partial_t (hu) + hu\partial_x u + u\partial_x (hu) + \partial_x (\frac{gh^2}{2}) = -gh\partial_x z, \end{cases}$$

where we used the chain rule for space derivatives. Therefore, the acoustic and transport systems are respectively given by

$$\begin{cases} \partial_t h + h\partial_x u = 0 \\ \partial_t (hu) + hu\partial_x u + \partial_x (\frac{gh^2}{2}) = -gh\partial_x z, \end{cases} \tag{2.1}$$

and

$$\partial_t X + u\partial_x X = 0 \tag{2.2}$$

with $X = h$ and $X = hu$. We also observe that the acoustic system (2.1) can be expressed as

$$\begin{cases} \partial_t \tau - \partial_m u = 0 \\ \partial_t u + \partial_m p = -\frac{g}{\tau}\partial_m z \end{cases} \tag{2.3}$$

where we have introduced the unknown $\tau = \frac{1}{h}$ and the mass variable m such that $\frac{1}{h}\partial_x = \partial_m$, see [14, 16–19]. Moreover, it is easy to find that the eigenvalues of system (2.3) are $\pm h\sqrt{gh} = \pm hc$.

About the Exner equation. Let us now consider the Exner equation as well, for which one could imagine at least three possibilities for numerical treatment. The first one would account for it at the acoustic level, the second one directly inside the transport step, and the third one by splitting it inside both steps. However, the issue of coupling the Exner equation and the shallow water system has been vastly studied in the literature. In particular, it is known that a fully decoupled scheme can lead to a numerical method which produces spurious oscillations inside the numerical solutions; this

issue has been clearly presented in [21]. Nevertheless, in many industry codes, decoupled approaches are still exploited, also due to the fact that they are easier to implement. However, it is not even necessary to consider a fully coupled scheme in order to avoid this problem; indeed a weak coupling of the equations at the numerical level can lead to satisfying results, see for instance [5]. In the latter, a three-wave approximate Riemann solver has been described and then re-interpreted as a splitting strategy. Moreover, they stated that one change in the fluid solver (there, the value of the wave speed in the approximate Riemann solver) can give place to splitting methods without spurious oscillations. We also refer to [35], where a weakly coupled method based on the HLL scheme is presented. Another possible reference is [34] in which the authors describe two methods based on the Roe approach. In this paper, they present not only a decoupled approach where the oscillations are partly stabilized by controlling the stability region, but also a fully-coupled scheme. Indeed, progresses to obtain fully coupled method for the Shallow Water Exner (SWExner) system have also been made. See for instance [12], where the authors describe a path-conservative Roe method and its high-order extension together with flux limiters, or [13] where Roe-type schemes have been extended to second-order of accuracy using a new MUSCL-type reconstruction. For additional references for both fully and weakly coupled methods, see for instance [4,10,20,29,30,40]. In this work we will mainly focus on weakly coupled numerical approach. Moreover, in the following we completely take into account the Exner equation in the transport (projection) step. Indeed, this work should be interpreted as a first step to understand how to treat the Exner equation in the Lagrange-projection framework. Thus, new strategies to include the Exner equation at the acoustic level or in both steps will be treated successively in the next work.

Finally, in the first part of this work, the acoustic and transport systems respectively read

$$\begin{cases} \partial_t \tau - \partial_m u = 0 \\ \partial_t u + \partial_m p = -\frac{g}{\tau}\partial_m z \\ \partial_t z = 0 \end{cases} \tag{2.4}$$

and

$$\begin{cases} \partial_t h + u\partial_x h = 0 \\ \partial_t (hu) + u\partial_x (hu) = 0 \\ \partial_t z + \zeta \partial_x q_b = 0. \end{cases} \tag{2.5}$$

Hence, the numerical strategy will be composed of two steps:

(1) Take into account the acoustic effects of the model and the topography spatial variations by solving system (2.4);

(2) Consider and solve the transport system (2.5).

System (1.1) in Lagrangian coordinates. In order to interpret the strategy as a Lagrange-Projection one, we first define the fluid particle ξ and the characteristic curves

$$\begin{cases} \frac{\partial x}{\partial t}(\xi,t) = u(x(\xi,t),t) \\ x(\xi,0) = \xi \end{cases} \tag{2.6}$$

which define the trajectory $: t \to x(\xi,t)$, of ξ as the time goes on. Therefore, any function $: (x,t) \to \varphi(x,t)$ in Eulerian coordinates can be written in Lagrangian coordinates,

$$\bar{\varphi}(\xi,t) = \varphi(x(\xi,t),t).$$

Let us now introduce the volume ratio

$$L(\xi,t)=\frac{\partial x}{\partial \xi}(\xi,t) \tag{2.7}$$

such that

$$\begin{cases} \frac{\partial L}{\partial t}(\xi,t)=\partial_\xi u(x(\xi,t),t) \\ L(\xi,0)=1. \end{cases} \tag{2.8}$$

Consequently, we note that

$$\partial_t L(\xi,t)=\partial_\xi u(x(\xi,t),t)=\partial_\xi \bar{u}(\xi,t),$$

and thus

$$\partial_\xi \bar{\varphi}(\xi,t)=L(\xi,t)\partial_x\varphi(x,t) \quad \text{and} \quad \partial_t\bar{\varphi}(\xi,t)=\partial_t\varphi(x,t)+u(x,t)\partial_x\varphi(x,t).$$

We have now all the ingredients to write (1.1) in Lagrangian coordinates. More precisely, observing that smooth solutions of (1.1) satisfy

$$\begin{cases} L(\partial_t h+u\partial_x h+h\partial_x u)=0 \\ L(\partial_t(hu)+u\partial_x(hu)+hu\partial_x u+\partial_x p+gh\partial_x z)=0 \end{cases}$$

and

$$\begin{cases} L\partial_t\bar{h}+\bar{h}\partial_t L=0 \\ L\partial_t\overline{hu}+\overline{hu}\partial_t L+\partial_\xi\bar{p}+g\bar{h}\partial_\xi\bar{z}=0 \end{cases}$$

we get

$$\begin{cases} \partial_t(L\bar{h})=0 \\ \partial_t(L\overline{hu})+\partial_\xi\bar{p}=-g\bar{h}\partial_\xi\bar{z}. \end{cases} \tag{2.9}$$

Notice that in the following sections, we shall omit the bar over the Lagrangian functions when there can be no confusion. This new formulation of system (1.1) exploiting the Lagrangian coordinates makes the above numerical strategy based on an acoustic-transport splitting strictly equivalent to a Lagrangian-projection splitting, that can be summarized as in the following,

(1) Solve system (2.9) in Lagrangian coordinates;

(2) Project the solution into Eulerian coordinates.

To conclude this section, we derive from (2.9) an evolution equation for Lu that will be useful in the next sections. Removing the bars and using the discharge equation on Lu, we have in particular

$$h\partial_t(Lu)+Lu\partial_t h+\partial_\xi p+gh\partial_\xi z=0$$

and, since $0=\partial_t(Lh)=h\partial_t L+L\partial_t h=h\partial_\xi u+L\partial_t h$, we get

$$h\partial_t(Lu)-hu\partial_\xi u+\partial_\xi p+gh\partial_\xi z=0$$

and finally

$$\partial_t(Lu)-\partial_\xi\frac{u^2}{2}=-g\partial_\xi(h+z). \tag{2.10}$$

Note that the source term now involves the quantity $h+z$ which is constant for stationary solutions.

2.1. A well-balanced approximate Riemann solver for the acoustic system. In this section we briefly recall the definition of a well-balanced approximate Riemann solver proposed in [19] for the acoustic system (2.4) and that will be useful in the following. It is based on the Gallice theory [25,26] which is an extension to balance laws of the Harten, Lax and van Leer formalism [28] for conservation laws. For more details about this Riemann solver, the reader can refer to [19]. Then, suppose that we want to solve (2.4) with the following Riemann initial data

$$\mathbf{U}(m,t=0)=\begin{cases}\mathbf{U}_L & \text{if} \quad m<0\\ \mathbf{U}_R & \text{if} \quad m\geq 0\end{cases}$$

where we have set

$$\mathbf{U}_L=\begin{pmatrix}\tau_L\\ u_L\\ z_L\end{pmatrix} \quad \text{and} \quad \mathbf{U}_R=\begin{pmatrix}\tau_R\\ u_R\\ z_R\end{pmatrix}.$$

The proposed approximate solution has the following form

$$\hat{\mathbf{U}}(\frac{m}{t};\mathbf{U}_L,\mathbf{U}_R)=\begin{cases}\mathbf{U}_L & \text{if} \quad \frac{m}{t}<-a\\ \mathbf{U}_L^* & \text{if} \quad -a<\frac{m}{t}<0\\ \mathbf{U}_R^* & \text{if} \quad 0<\frac{m}{t}<a\\ \mathbf{U}_R & \text{if} \quad \frac{m}{t}>a\end{cases}$$

where a is a constant and where the intermediate states

$$\mathbf{U}_L^*=\begin{pmatrix}\tau_L^*\\ u_L^*\\ z_L\end{pmatrix}, \quad \mathbf{U}_R^*=\begin{pmatrix}\tau_R^*\\ u_R^*\\ z_R\end{pmatrix} \tag{2.11}$$

are defined thanks to

$$\begin{cases}\tau_{*,L}=\tau_L+\dfrac{1}{a}(u_*-u_L)\\ \tau_{*,R}=\tau_R-\dfrac{1}{a}(u_*-u_R)\\ u_L^*=u_R^*=u^*\\ u^*=\dfrac{1}{2}(u_L+u_R)-\dfrac{1}{2a}(\Pi_R-\Pi_L)-\dfrac{\mathcal{M}}{2a}\\ \Pi^*=\dfrac{1}{2}(\Pi_L+\Pi_R)-\dfrac{a}{2}(u_R-u_L)\end{cases}$$

with

$$\mathcal{M}=\frac{g}{2}(\frac{1}{\tau_L}+\frac{1}{\tau_R})(z_R-z_L).$$

Observe that Π is a new variable introduced to be able to define the approximate Riemann solver. In particular, Π can be interpreted as a linearization of the pressure term p and its initial data are well-prepared in the sense that $\Pi=p$.

Then, it is clear that $\mathcal{M}=0$ if $z_L=z_R$ so that the classical form of an approximate Riemann solver for a system of conservation laws is recovered, while $X_L^*=X_L$ and

$X_R^* = X_R$ with $X = \tau, u$, when the "lake at rest" stationary conditions are satisfied, namely

$$u_L = u_R = 0, \quad h_L + z_L = h_R + z_R.$$

In that sense, the proposed approximate Riemann solver is said to be well-balanced. Note that this is true whatever the definition of the constant a is. In practice, we will choose $a = \max((hc)_L, (hc)_R)$ according the well-known subcharacteristic stability condition. For more details, we refer again to [19].

3. Numerical methods

Before getting into the heart of the matter, we give a few details about the time and space discretizations we use in the following sections. Given a constant time step Δt, we define the intermediate times by $t^n = n\Delta t$ for $n \in \mathbb{N}$. Then, the mesh interfaces are $x_{j+1/2} = j\Delta x$ for $j \in \mathbb{Z}$, where Δx is the constant space step, while x_j is the center of the cell $[x_{j-1/2}, x_{j+1/2})$. Hence, given a variable φ, we denote φ_j^n its constant average approximation on each cell $[x_{j-1/2}, x_{j+1/2})$ at time t^n, namely

$$\varphi_j^n \approx \frac{1}{\Delta x} \int_{x_{j-1/2}}^{x_{j+1/2}} \varphi(x, t^n)\, dx,$$

with $n \in \mathbb{N}$ and $j \in \mathbb{Z}$. At last, note that, regarding the mass variable m, we use $\Delta m_j = h_j^n \Delta x$ for all j.

Given the sequence $\{\varphi_j^n\}_j$, we now look for its approximation at the next time level t^{n+1}, namely $\{\varphi_j^{n+1}\}_j$. At this stage, we are able to present the numerical schemes, starting with the first-order method and proceeding with the second-order one. For each of them, we will prove the well-balanced condition as well. Let us recall that the numerical schemes are divided into two different steps. First we have the acoustic step, in which we numerically solve system (2.4). Then, we exploit its solution as initial condition for solving system (2.5). We can sum up this procedure in the following way,

(1) Acoustic step: solve system (2.4) in order to update $\mathbf{Q}^n$ to $\mathbf{Q}^{n+1-}$;
(2) Transport step: find $\mathbf{Q}^{n+1}$ from $\mathbf{Q}^{n+1-}$ by the approximation of the solution of system (2.5).

Note that in the first step, we implicitly use the change of variable $\mathbf{U} = \mathbf{U}(\mathbf{Q})$ to first define $\mathbf{U}^n$ from $\mathbf{Q}^n$ before solving (2.4), and then the change of variables $\mathbf{Q} = \mathbf{Q}(\mathbf{U})$ to define $\mathbf{Q}^{n+1-}$ from $\mathbf{U}^{n+1-}$.

3.1. First-order scheme.

Here we give the details for the first-order scheme distinguishing between the acoustic and transport steps.

3.1.1. Acoustic step and Lagrangian reformulation.

As far as the discretization of (2.4) is concerned, we suggest to use a classical Godunov-type method based on the well-balanced approximate Riemann solver proposed in Section 2.1. As usual, it simply consists in averaging on each cell the juxtaposition of the approximate Riemann solutions set at each interface. Therefore, it follows after easy calculations that the numerical discretization of the acoustic relaxation system (2.4) can be formulated as

$$\begin{cases} \tau_j^{n+1-} = \tau_j^n + \frac{\Delta t}{\Delta m_j}(u^*_{j+\frac{1}{2}} - u^*_{j-\frac{1}{2}}) \\ u_j^{n+1-} = u_j^n - \frac{\Delta t}{\Delta m_j}(\Pi^*_{j+\frac{1}{2}} - \Pi^*_{j-\frac{1}{2}}) - \Delta t \{\frac{g}{\tau}\partial_m z\}_j^n \end{cases} \tag{3.1}$$

where we have set

$$\begin{aligned} u^*_{j+\frac{1}{2}} &= u^*_{j+\frac{1}{2}}(\mathbf{Q}^n_j, \mathbf{Q}^n_{j+1}) = \frac{1}{2}(u^n_{j+1} + u^n_j) - \frac{1}{2a^n_{j+\frac{1}{2}}}(\Pi^n_{j+1} - \Pi^n_j) - \frac{\mathcal{M}^n_{j+1/2}}{2a_{j+1/2}} \\ \Pi^*_{j+\frac{1}{2}} &= \Pi^*_{j+\frac{1}{2}}(\mathbf{Q}^n_j, \mathbf{Q}^n_{j+1}) = \frac{1}{2}(\Pi^n_{j+1} + \Pi^n_j) - \frac{a^n_{j+\frac{1}{2}}}{2}(u^n_{j+1} - u^n_j), \end{aligned} \tag{3.2}$$

$a^n_{j+\frac{1}{2}} = \max((hc)^n_j, (hc)^n_{j+1})$, while regarding the source term, we have

$$\{\frac{g}{\tau}\partial_m z\}^n_j = \frac{1}{2}\Big(\frac{\Delta m_{j+1/2}}{\Delta m_j}\{\frac{g}{\tau}\partial_m z\}^n_{j+1/2} + \frac{\Delta m_{j-1/2}}{\Delta m_j}\{\frac{g}{\tau}\partial_m z\}^n_{j-1/2}\Big) \tag{3.3}$$

where $\Delta m_{j+1/2} = (\Delta m_j + \Delta m_{j+1})/2$, $\Delta m_j = \frac{\tau^n_j}{\Delta x}$ and

$$\{\frac{g}{\tau}\partial_m z\}^n_{j+1/2} = \frac{\mathcal{M}^n_{j+1/2}}{\Delta m_{j+1/2}} \quad \text{with} \quad \mathcal{M}_{j+1/2} = \frac{g}{2}(\frac{1}{\tau^n_j} + \frac{1}{\tau^n_{j+1}})(z^n_{j+1} - z^n_j) \quad \forall j.$$

Let us note that z remains constant in this step, thus $z^{n+1-}_j = z^n_j$ for all j.

Lagrangian reformulation of (3.1). Let us observe that (3.1) reveals to be strictly equivalent to

$$\begin{cases} L^{n+1-}_j h^{n+1-}_j = L^n_j h^n_j \\ L^{n+1-}_j (hu)^{n+1-}_j = L^n_j (hu)^n_j - \frac{\Delta t}{\Delta x}(\Pi^*_{j+\frac{1}{2}} - \Pi^*_{j-\frac{1}{2}}) + \Delta t s^n_j \end{cases} \tag{3.4}$$

where we have set

$$L^{n+1-}_j = L^n_j + \frac{\Delta t}{\Delta x}(u^*_{j+\frac{1}{2}} - u^*_{j-\frac{1}{2}}) \quad \text{with} \quad L^n_j = 1 \tag{3.5}$$

and

$$s = -gh\partial_x z, \quad s^n_j = \frac{1}{2}\Big(s^n_{j+1/2} + s^n_{j-1/2}\Big) \quad \text{and} \quad s^n_{j+1/2} = -\frac{\mathcal{M}^n_{j+1/2}}{\Delta x} \quad \forall j.$$

Considering that the Lagrangian variable ξ is discretized using the same mesh step as the one we used for x, namely $\Delta\xi = \Delta x$, and $\xi_{j+1/2} = x_{j+1/2}$, $\xi_j = x_j$ for all j, it is clear that (3.4) and (3.5) respectively approximate (2.9) and (2.8). This Lagrangian reformulation turns out to be crucial in order to derive hereafter a second-order extension of the propose numerical scheme. Note that we still have of course $z^{n+1-}_j = z^n_j$ for all j.

3.1.2. Projection step. As already mentioned, the aim of this step is to turn into Eulerian coordinates the solution obtained at the end of the previous step, thanks to (3.4) and given in Lagrangian coordinates. This amounts to solving the transport system (2.5) which also contains the evolution equation for z. Recall indeed that z stayed constant in the first step.

In order to project $X = h, hu$ on the Eulerian grid, we use the following identity

$$\int_{\xi_1}^{\xi_2} L(\xi,t)X(\xi,t)d\xi = \int_{x(\xi_1,t)}^{x(\xi_2,t)} X(x,t)dx$$

where we recall that the trajectories $t \mapsto x(\xi,t)$ and the volume ratio $L(\xi,t)$ are defined by (2.6) and (2.7). Therefore, it is natural to define $\hat{\xi}_{j+1/2}$ such that $x(\hat{\xi}_{j+1/2},t^{n+1}) = x_{j+1/2}$ and $x(\hat{\xi}_{j+1/2},t^n) = \hat{\xi}_{j+1/2}$ for all j and to write

$$X_j^{n+1} = \frac{1}{\Delta x}\int_{x_{j-\frac{1}{2}}}^{x_{j+\frac{1}{2}}} X(x,t^{n+1})dx = \frac{1}{\Delta x}\int_{x(\hat{\xi}_{j-\frac{1}{2}},t^{n+1})}^{x(\hat{\xi}_{j+\frac{1}{2}},t^{n+1})} X(x,t^{n+1})dx$$
$$= \frac{1}{\Delta x}\int_{\hat{\xi}_{j-\frac{1}{2}}}^{\hat{\xi}_{j+\frac{1}{2}}} L(\xi,t^{n+1-})X(\xi,t^{n+1-})d\xi. \tag{3.6}$$

Splitting the last integral into three parts, namely

$$X_j^{n+1} = \frac{1}{\Delta x}\int_{\hat{\xi}_{j-\frac{1}{2}}}^{\xi_{j-\frac{1}{2}}} L(\xi,t^{n+1-})X(\xi,t^{n+1-})d\xi +$$
$$+ \frac{1}{\Delta x}\int_{\xi_{j-\frac{1}{2}}}^{\xi_{j+\frac{1}{2}}} L(\xi,t^{n+1-})X(\xi,t^{n+1-})d\xi + \frac{1}{\Delta x}\int_{\xi_{j+\frac{1}{2}}}^{\hat{\xi}_{j+\frac{1}{2}}} L(\xi,t^{n+1-})X(\xi,t^{n+1-})d\xi, \tag{3.7}$$

and approximating $\hat{\xi}_{j+1/2}$ by

$$x_{j+1/2} = x(\hat{\xi}_{j+1/2},t^{n+1}) \simeq x(\hat{\xi}_{j+1/2},t^n) + \Delta t \partial_t x(\hat{\xi}_{j+1/2},t^n) \simeq \hat{\xi}_{j+1/2} + \Delta t u^*_{j+1/2},$$

it is natural to set, using first-order approximations of the integrals,

$$X_j^{n+1} = \frac{\xi_{j-\frac{1}{2}} - \hat{\xi}_{j-\frac{1}{2}}}{\Delta x}(LX)^{n+1}_{j-1/2} + (LX)_j^{n+1-} + \frac{\hat{\xi}_{j+\frac{1}{2}} - \xi_{j+\frac{1}{2}}}{\Delta x}(LX)^{n+1}_{j+1/2} \tag{3.8}$$

where for all j

$$(LX)^{n+1}_{j+1/2} = \begin{cases} (LX)_j^{n+1-} & \text{if} \quad u^*_{j+1/2} \geq 0 \\ (LX)_{j+1}^{n+1-} & \text{if} \quad u^*_{j+1/2} < 0. \end{cases}$$

After easy manipulations, (3.8) is equivalent to

$$X_j^{n+1} = (LX)_j^{n+1-} - \frac{\Delta t}{\Delta x}\left(u^*_{j+\frac{1}{2}}(LX)^{n+1-}_{j+\frac{1}{2}} - u^*_{j-\frac{1}{2}}(LX)^{n+1-}_{j-\frac{1}{2}}\right). \tag{3.9}$$

Therefore, taking $X = h$ and $X = hu$ concludes the projection on the Eulerian grid.

Let us now consider the Exner equation for which we propose two different strategies. On one hand, we simply update the topography as in the following

$$z_j^{n+1} = z_j^n - \zeta\frac{\Delta t}{\Delta x}\left(u^*_{j+\frac{1}{2}}\left(\frac{q_b}{u}\right)^n_{j+\frac{1}{2}} - u^*_{j-\frac{1}{2}}\left(\frac{q_b}{u}\right)^n_{j-\frac{1}{2}}\right), \tag{3.10}$$

with

$$\left(\frac{q_b}{u}\right)^n_{j+1/2} = \begin{cases} \left(\frac{q_b}{u}\right)(u^n_{j+1}) & \text{if} \quad u^*_{j+\frac{1}{2}} \leq 0 \\ \left(\frac{q_b}{u}\right)(u^n_j) & \text{if} \quad u^*_{j+\frac{1}{2}} > 0, \end{cases}$$

where we see that the numerical fluxes are evaluated simply using the solution at time t^n, and not the one obtained at the end of the Lagrangian step. This means in some sense that the evolution of the topography is not coupled with the one hydrodynamic model from a numerical point of view and this is the reason why this strategy is said to be *decoupled*. At last, note that $\frac{q_b}{u}$ is well-defined in the sense that $q_b = 0$ if $u = 0$, as it is generally usual in the formulations for the solid transport discharge. On the other hand, we propose a *weakly coupled* strategy in which we exploit the solution obtained at time t^{n+1-}, by setting

$$z_j^{n+1} = z_j^n - \zeta \frac{\Delta t}{\Delta x}\left(u^*_{j+\frac{1}{2}}\left(\frac{q_b}{u}\right)^{n+1-}_{j+\frac{1}{2}} - u^*_{j-\frac{1}{2}}\left(\frac{q_b}{u}\right)^{n+1-}_{j-\frac{1}{2}}\right). \tag{3.11}$$

At this stage, notice that it would be tempting to define $\left(\frac{q_b}{u}\right)^{n+1-}_{j+\frac{1}{2}}$ using the velocity u^{n+1-} simply defined by $u^{n+1-} = \dfrac{Lhu^{n+1-}}{Lh^{n+1-}}$. However, even if this option results to be natural, dividing by Lh rises difficulties when considering the second-order extension. For this reason, we prefer to set

$$(\frac{q_b}{u})^{n+1-}_{j+1/2} = \begin{cases} (\frac{q_b}{u})\Big((Lu)^{n+1-}_{j+1}\Big) & \text{if} \quad u^*_{j+\frac{1}{2}} \le 0 \\ (\frac{q_b}{u})\Big((Lu)^{n+1-}_{j}\Big) & \text{if} \quad u^*_{j+\frac{1}{2}} > 0, \end{cases}$$

where a possible discretization of the evolution equation (2.10) for Lu reads

$$(Lu)_j^{n+1-} = (Lu)_j^n + \frac{\Delta t}{2\Delta x}((u^*_{j+\frac{1}{2}})^2 - (u^*_{j-\frac{1}{2}})^2) + \Delta t \frac{\hat{s}_{j+\frac{1}{2}} + \hat{s}_{j-\frac{1}{2}}}{2} \tag{3.12}$$

with

$$\hat{s}_{j+\frac{1}{2}} = -g\frac{(h+z)^n_{j+1} - (h+z)^n_j}{\Delta x}.$$

As a last remark we observe that, since we are also interested in a 2D formulation and (2.10) could not be extended in two dimensions as it is (see hereafter), we will propose an alternative approximation of Lu which reads

$$(Lu)_j^{n+1-} = (Lu)_j^n + \frac{u_j^n + u_{j+1}^n}{2}\frac{\Delta t}{\Delta x}(u^*_{j+\frac{1}{2}} - u^*_{j-\frac{1}{2}}) + \Delta t \frac{\hat{s}_{j+\frac{1}{2}} + \hat{s}_{j-\frac{1}{2}}}{2}.$$

Both formulations turn out to give the same results in 1D.

3.1.3. Overall scheme and well-balanced property. Next, we give an equivalent formulation of our first-order scheme which takes into account both the acoustic and transport steps. This formulation is interesting in the sense that it clearly shows that the scheme is indeed conservative when there is no source term. More precisely, considering together (3.4) and (3.9) we easily get

$$\begin{cases} h_j^{n+1} = h_j^n - \dfrac{\Delta t}{\Delta x}\left(u^*_{j+\frac{1}{2}}(Lh)^{n+1-}_{j+\frac{1}{2}} - u^*_{j-\frac{1}{2}}(Lh)^{n+1-}_{j-\frac{1}{2}}\right) \\ (hu)_j^{n+1} = (hu)_j^n - \dfrac{\Delta t}{\Delta x}\left(u^*_{j+\frac{1}{2}}(Lhu)^{n+1-}_{j+\frac{1}{2}} + \Pi^*_{j+\frac{1}{2}} - u^*_{j-\frac{1}{2}}(Lhu)^{n+1-}_{j-\frac{1}{2}} - \Pi^*_{j-\frac{1}{2}}\right) + \Delta t s_j^n \end{cases} \tag{3.13}$$

while the evolution Equations (3.10) and (3.11) for z are clearly conservative. Let us now prove the well-balanced property.

THEOREM 3.1. *The first-order numerical scheme with updating formula (3.13) and (3.10) or (3.11) preserves the "lake at rest" stationary solution (1.6).*

Proof. Assuming to be under the "lake at rest" condition, that is to say $u_j^n = 0$ and $h_j^n + z_j^n =$ constant for all j, it is straightforward to demonstrate that this stationary solution is preserved. Indeed, few algebraic computations show that $u^*_{j+\frac{1}{2}} = 0$ as $u_j^n = u_{j+1}^n = 0$ and

$$\Pi_{j+1}^n - \Pi_j^n = \frac{g}{2}((h_{j+1}^n)^2 - (h_j^n)^2) = \frac{g}{2}(h_j^n + h_{j+1}^n)(h_{j+1}^n - h_j^n) = -\frac{g}{2}(h_j^n + h_{j+1}^n)(z_{j+1}^n - z_j^n).$$

Similarly, it can be proved that $\frac{1}{\Delta x}(\Pi^*_{j+\frac{1}{2}} - \Pi^*_{j-\frac{1}{2}}) = s_j^n$ and thus $(Lhu)_j^{n+1-} = (Lhu)_j^n = (hu)_j^n = 0$. We can also note that $(Lu)_j^{n+1-} = 0$ as $(h+z)_j^n = (h+z)_{j+1}^n$ for all j. Finally, it is easily seen that under the property $u^*_{j+1/2} = 0$ for all j, the transport step gives $h_j^{n+1} = h_j^n$, $(hu)_j^{n+1} = 0$ and $z_j^{n+1} = z_j^n$, which concludes the proof. ∎

3.2. Second-order scheme. We now explain how to reach the second order of accuracy in both space and time. While increasing the order of accuarcy is a standard process, the key issue is to preserve the well-balanced property.

In order to construct a high-order approximation in space, we will make use of classical first-order polynomial reconstructions, but applied to the so-called fluctuations, which is non-standard and has been introduced in [39] to combine both the well-balanced property and the higher order property.

Regarding the second-order discretization in time, we simply consider Runge-Kutta TVD scheme at second order [27]. In particular, we apply it to the overall scheme (Lagrangian and remap step together) in order to avoid diffusion due to the splitting.

3.2.1. Lagrangian step. In order to reach the second order of accuracy in space, we begin by defining at time t^n and for each cell j a stationary solution denoted by $x \mapsto \mathbf{Q}_j^{n,e}(x)$ and defined for all x by

$$\left(h_j^{n,e}\right)(x) = h_j^n + z_j^n - z^n(x), \quad u_j^{n,e}(x) = u_j^n \quad \text{and} \quad z_j^{n,e}(x) = z^n(x), \tag{3.14}$$

where $x \mapsto z^n(x)$ is nothing but the piecewise constant approximation of z at time t^n, namely such that $z^n(x) = z_j^n$ for all x in $[x_{j-1/2}, x_{j+1/2})$. Such a reconstructed solution satisfies the in-cell conservation property

$$\frac{1}{\Delta x}\int_{x_{j-\frac{1}{2}}}^{x_{j+\frac{1}{2}}} \mathbf{Q}_j^{n,e}(x)dx = \mathbf{Q}_j^n.$$

Next, we follow [39] and introduce the so-called j-fluctuations defined as

$$\mathbf{D}_{k,j}^n = \mathbf{Q}_k^n - \frac{1}{\Delta x}\int_{x_{k-1/2}}^{x_{k+1/2}} \mathbf{Q}_j^{n,e}(x)dx,$$

for all k. Observe that $\mathbf{D}_{j,j}^n = \mathbf{0}$ by construction, while $\mathbf{D}_{k,j}^n = \mathbf{0}$ for all k if the approximate solution at time t^n satisfies the "lake at rest" condition (1.6).

At last, for each cell I_j we make use of a reconstructed polynomial vector $\mathbf{P}_j^n(x)$ defined by

$$\mathbf{P}_j^n(x) = \mathbf{Q}_j^n + \Delta_j^n(x - x_j),$$

where $\Delta_j^n = \Delta_j^n(\mathbf{D}_{j-1,j}^n, \mathbf{D}_{j,j}^n, \mathbf{D}_{j+1,j}^n)$ is the ENO [43] or the MINMOD [42] slope applied to the fluctuations.

The numerical fluxes $u^*_{j+\frac{1}{2}}$ and $\Pi^*_{j+\frac{1}{2}}$ are then defined in a very classical way using the interfaces values

$$\mathbf{Q}^n_{j+\frac{1}{2}L} = \mathbf{P}^n_j(x_{j+\frac{1}{2}}) \quad \text{and} \quad \mathbf{Q}^n_{j+\frac{1}{2}R} = \mathbf{P}^n_{j+1}(x_{j+\frac{1}{2}}),$$

and formula (3.2), namely

$$u^*_{j+\frac{1}{2}} = u^*_{j+\frac{1}{2}}(\mathbf{Q}^n_{j+\frac{1}{2}L}, \mathbf{Q}^n_{j+\frac{1}{2}R}) \quad \text{and} \quad \Pi^*_{j+\frac{1}{2}} = \Pi^*_{j+\frac{1}{2}}(\mathbf{Q}^n_{j+\frac{1}{2}L}, \mathbf{Q}^n_{j+\frac{1}{2}R}), \tag{3.15}$$

with

$$a^n_{j+\frac{1}{2}} = \max\left(h^n_{j+\frac{1}{2},L} c^n_{j+\frac{1}{2},L}, h^n_{j+\frac{1}{2},R} c^n_{j+\frac{1}{2},R}\right).$$

Regarding the source term, once again we exploit formulas (3.3). Let us note that, thanks to formula (3.14), $z_{j+\frac{1}{2}L} = z_j$ and $z_{j+\frac{1}{2}R} = z_{j+1}$ as the fluctuations related to the topography are null. Finally, the discretization of the Lagrangian system (2.9) reads as in the first-order step, namely

$$\begin{cases} L_j^{n+1-} h_j^{n+1-} = L_j^n h_j^n \\ L_j^{n+1-} (hu)_j^{n+1-} = L_j^n (hu)_j^n - \frac{\Delta t}{\Delta x}(\Pi^*_{j+\frac{1}{2}} - \Pi^*_{j-\frac{1}{2}}) + \Delta t s_j^n. \end{cases}$$

3.2.2. Projection step. In this step, we exploit again a reconstructed polynomial **LP**. However, in order to preserve the second-order of accuracy, it is crucial to reconstruct the Lagrangian variables (LX), namely as

$$(LX)_j^{n+1-}(\xi) = (LX)_j^{n+1-} + \Delta_j^{n+1-}(\xi - \xi_j) \tag{3.16}$$

with the slope $\Delta_j^{n+1-} = \Delta_j^{n+1-}((LX)_{j-1}^{n+1-}, (LX)_j^{n+1-}, (LX)_{j+1}^{n+1-})$ and where the variable X denotes h, hu and u. Then, the updating formula for $X = h$ and $X = hu$ are given by a second-order approximation of the three integrals that appear in (3.7). This is achieved by using the mid-point rule, thus we get

$$\begin{aligned} X_j^{n+1-} = (LX)_j^{n+1-} - \frac{\Delta t}{\Delta x}\Big(u^*_{j+\frac{1}{2}} (LX)^{n+1-}_{j+\frac{1}{2}}\Big(\frac{\xi_{j+\frac{1}{2}} + \hat{\xi}_{j+\frac{1}{2}}}{2}\Big) + \\ - u^*_{j-\frac{1}{2}} (LX)^{n+1-}_{j-\frac{1}{2}}\Big(\frac{\xi_{j-\frac{1}{2}} + \hat{\xi}_{j-\frac{1}{2}}}{2}\Big)\Big), \end{aligned} \tag{3.17}$$

where we use the upwind definition

$$(LX)^{n+1-}_{j-\frac{1}{2}}(\xi) = \begin{cases} (LX)^{n+1-}_{j-1}(\xi) & \text{if} \quad u^*_{j-\frac{1}{2}} > 0 \\ (LX)^{n+1-}_{j}(\xi) & \text{if} \quad u^*_{j-\frac{1}{2}} \leq 0. \end{cases} \tag{3.18}$$

As far as the topography is concerned, we consider the weakly coupled scheme (3.11) where we naturally set

$$\left(\frac{q_b}{u}\right)^{n+1-}_{j+1/2} = \begin{cases} \left(\frac{q_b}{u}\right)\Big((Lu)^{n+1-}_{j+1}\left(\frac{\xi_{j+\frac{1}{2}} + \hat{\xi}_{j+\frac{1}{2}}}{2}\right)\Big) & \text{if} \quad u^*_{j+\frac{1}{2}} \leq 0 \\ \left(\frac{q_b}{u}\right)\Big((Lu)^{n+1-}_{j}\left(\frac{\xi_{j+\frac{1}{2}} + \hat{\xi}_{j+\frac{1}{2}}}{2}\right)\Big) & \text{if} \quad u^*_{j+\frac{1}{2}} > 0, \end{cases}$$

and $u^*_{j\pm\frac{1}{2}}$ is given by (3.15).

Afterwards, for the decoupled scheme, we first define the reconstructed polynomial for the water height h and the flow hu at time t^n,

$$P(X)^n_j(x) = X^n_j + \Delta^n_j(x - x_j)$$

with $X = h, hu$ and Δ^n_j the slopes (either ENO or Minmod). Then, we use formula (3.10) where we impose

$$\left(\frac{q_b}{u}\right)^n_{j+1/2} = \begin{cases} \left(\frac{q_b}{u}\right)\left(\frac{P(hu)^n_{j+1}(x_{j+\frac{1}{2}})}{P(h)^n_{j+1}(x_{j+\frac{1}{2}})}\right) & \text{if} \quad u^*_{j+\frac{1}{2}} \le 0 \\ \left(\frac{q_b}{u}\right)\left(\frac{P(hu)^n_{j}(x_{j+\frac{1}{2}})}{P(h)^n_{j}(x_{j+\frac{1}{2}})}\right) & \text{if} \quad u^*_{j+\frac{1}{2}} > 0. \end{cases}$$

THEOREM 3.2. *The second-order numerical scheme described preserves the "lake at rest" stationary solution (1.6).*

Proof. Since we already proved the well-balanced property for the first-order scheme, it is straightforward to show it for the second-order method as well. Indeed, it is enough to observe that the slopes $\Delta^n_j = \Delta^n_j(\mathbf{D}^n_{j-1,j}, \mathbf{D}^n_{j,j}, \mathbf{D}^n_{j+1,j})$ are null under the hypothesis of the "lake at rest condition" thanks to definition of the fluctuations. Hence, once again we obtain $u^*_{j+\frac{1}{2}} = 0$ and thus $Lhu^{n+1-}_j = hu^n_j = 0$, $Lh^{n+1-}_j = h^n_j$, $hu^{n+1}_j = Lhu^{n+1-}_j = hu^n_j = 0$, $h^{n+1}_j = Lh^{n+1-}_j = h^n_j$ and $z^{n+1}_j = z^n_j$. Finally, it is only worth to specify that the Runge-Kutta TVD procedure automatically preserves the stationary solutions. ∎

4. Two-dimensional extension

In this section, we briefly describe how we extend the proposed approach in two space dimensions using dimensional splitting. Let us first recall that if we denote $(x,y) \in \mathbb{R}^2$ the space variables and $\mathbf{u} = (u,v)^T$ the velocity vector, then the 2D shallow water system reads

$$\begin{cases} \partial_t h + \nabla \cdot (h\mathbf{u}) = 0 \\ \partial_t (h\mathbf{u}) + \nabla \cdot (h\mathbf{u} \otimes \mathbf{u}) + \nabla p = -gh\nabla z, \end{cases} \tag{4.1}$$

while the Exner equation is given by

$$\partial_t z + \zeta \partial_x q_{b,x} + \zeta \partial_y q_{b,y} = 0$$

where $q_{b,x}$ and $q_{b,y}$ are the solid transport discharges in the x and y directions respectively. Exploiting once again the Grass model, their formula are the following,

$$q_{b,x} = A_g u(u^2 + v^2) \quad \text{and} \quad q_{b,y} = A_g v(u^2 + v^2).$$

Notice that the "lake at rest" stationary solutions now satisfy

$$u = 0, \quad v = 0 \quad \text{and} \quad \nabla(h + z) = 0.$$

It is still possible to consider a Lagrangian formulation of these equations. More precisely, let us introduce the Lagrangian coordinates (ξ_1, ξ_2) and consider the map $: (\xi_1, \xi_2) \to (x,y)$, with $x = x(\xi_1, \xi_2, t)$, $y = y(\xi_1, \xi_2, t)$ and such that

$$\frac{\partial x}{\partial t} = u(x,y,t) \quad \text{and} \quad \frac{\partial y}{\partial t} = v(x,y,t),$$

$$x(\xi_1,\xi_2,0)=\xi_1, \quad y(\xi_1,\xi_2,0)=\xi_2.$$

We also assume that for each $t>0$, this map is invertible and its Jacobian (determinant of the Jacobian matrix) is given by

$$L(\xi_1,\xi_2,t)=\begin{vmatrix}\partial_{\xi_1}x & \partial_{\xi_2}x\\ \partial_{\xi_1}y & \partial_{\xi_2}y\end{vmatrix}$$

with $L(\xi_1,\xi_2,0)=1$ and, after easy calculations,

$$\frac{\partial L(\xi_1,\xi_2,t)}{\partial t}=L\nabla\cdot\mathbf{u}=L\partial_x u+L\partial_y v. \tag{4.2}$$

Then, it can be shown that the Lagrangian formulation of the system writes

$$\begin{cases}\partial_t(Lh)=0\\ \partial_t(Lh\mathbf{u})+L\nabla p=-ghL\nabla z,\end{cases} \tag{4.3}$$

where the gradient is still taken with respect to the Eulerian variables (x,y), while on the other hand we also have

$$\partial_t(L\mathbf{u})-\mathbf{u}L\nabla\cdot\mathbf{u}+gL\nabla(h+z)=0,$$

which will be useful hereafter. We refer the reader to [32, 33] for more details about Lagrangian coordinates in 2-dimensions.

We now give the basic formulas based on a dimensional splitting and introduce some notations. First of all, the computational domain $\Omega\subset\mathbb{R}$ is divided into $M_x\times M_y$ rectangular cells with constant space steps Δx and Δy in the x and y directions respectively. Then, the mesh interfaces are given by $x_{i+1/2}$ for $i\in\{0,\dots,M_x\}$ and $y_{j+1/2}$ for $j\in\{0,\dots,M_y\}$. Thus, $\varphi_{i,j}^n$ denotes the piecewise constant approximation of the variable φ in the cell $[x_{i-1/2},x_{i+1/2})\times[y_{j-1/2},y_{j+1/2})$ at time t^n, namely

$$\varphi_{i,j}^n\approx\frac{1}{\Delta x}\int_{x_{i-1/2}}^{x_{i+1/2}}\int_{y_{j-1/2}}^{y_{j+1/2}}\varphi(x,y,t^n)\,dx\,dy.$$

Acoustic step. Following the 1D scheme, the numerical approximation of (4.3) is taken to be

$$\begin{cases}(Lh)_{i,j}^{n+1-}=(Lh)_{i,j}^n\\ (Lhu)_{i,j}^{n+1-}=(Lhu)_{i,j}^n-\dfrac{\Delta t}{\Delta x}(\Pi^*_{i+\frac12,j}-\Pi^*_{i-\frac12,j})+\Delta t s_{i,j}^{1,n}\\ (Lhv)_{i,j}^{n+1-}=(Lhv)_{i,j}^n-\dfrac{\Delta t}{\Delta y}(\Pi^*_{i,j+\frac12}-\Pi^*_{i,j-\frac12})+\Delta t s_{i,j}^{2,n}\end{cases} \tag{4.4}$$

where we have set

$$L_{i,j}^{n+1-}=L_{i,j}^n+\frac{\Delta t}{\Delta x}(u^*_{i+\frac12,j}-u^*_{i-\frac12,j})+\frac{\Delta t}{\Delta y}(v^*_{i,j+\frac12}-v^*_{i,j-\frac12}) \tag{4.5}$$

with

$$\begin{aligned}
u^*_{i+\frac{1}{2},j} &= \frac{1}{2}(u^n_{i+1,j}+u^n_{i,j}) - \frac{1}{2a^n_{i+\frac{1}{2},j}}(\Pi^n_{i+1,j}-\Pi^n_{i,j}) - \frac{\mathcal{M}^n_{i+1/2,j}}{2a_{i+1/2,j}},\\
v^*_{i,j+\frac{1}{2}} &= \frac{1}{2}(v^n_{i,j+1}+v^n_{i,j}) - \frac{1}{2a^n_{i,j+\frac{1}{2}}}(\Pi^n_{i,j+1}-\Pi^n_{i,j}) - \frac{\mathcal{M}^n_{i,j+1/2}}{2a_{i,j+1/2}},\\
\Pi^*_{i+\frac{1}{2},j} &= \frac{1}{2}(\Pi^n_{i+1,j}+\Pi^n_{i,j}) - \frac{a^n_{i+\frac{1}{2},j}}{2}(u^n_{i+1,j}-u^n_{i,j}),\\
\Pi^*_{i,j+\frac{1}{2}} &= \frac{1}{2}(\Pi^n_{i,j+1}+\Pi^n_{i,j}) - \frac{a^n_{i,j+\frac{1}{2}}}{2}(v^n_{i,j+1}-v^n_{i,j}),
\end{aligned} \tag{4.6}$$

with $a^n_{i+1/2,j}=\max((hc)^n_{i,j},(hc)^n_{i+1,j})$, $a^n_{i,j+1/2}=\max((hc)^n_{i,j},(hc)^n_{i,j+1})$, while regarding the source term, we have for all j

$$\begin{aligned}
s^{1,n}_{i,j} &= \frac{1}{2}\left(s^n_{i+1/2,j}+s^n_{i-1/2,j}\right) \quad \text{with} \quad s^n_{i+1/2,j} = -\frac{\mathcal{M}^n_{i+1/2,j}}{\Delta x}\\
s^{2,n}_{i,j} &= \frac{1}{2}\left(s^n_{i,j+1/2}+s^n_{i,j-1/2}\right) \quad \text{with} \quad s^n_{i,j+1/2} = -\frac{\mathcal{M}^n_{i,j+1/2}}{\Delta y}
\end{aligned}$$

with

$$\mathcal{M}^n_{i+1/2,j} = \frac{g}{2}\left(\frac{1}{\tau^n_{i,j}}+\frac{1}{\tau^n_{i+1,j}}\right)(z^n_{i+1,j}-z^n_{i,j}), \quad \mathcal{M}^n_{i,j+1/2} = \frac{g}{2}\left(\frac{1}{\tau^n_{i,j}}+\frac{1}{\tau^n_{i,j+1}}\right)(z^n_{i,j+1}-z^n_{i,j}).$$

It is clear that the numerical scheme (4.6) is a natural extension of the one used for the one-dimensional system.

Projection step. As before, the second step of the Lagrange-projection scheme consists in projecting the solution obtained at the end of the acoustic step onto the Eulerian grid, that is to say in approximating the transport system

$$\partial_t\varphi + \mathbf{u}\cdot\nabla\varphi = 0$$

or equivalently

$$\partial_t\varphi + \nabla\cdot(\varphi\mathbf{u}) - \varphi\nabla\cdot\mathbf{u} = 0,$$

where we assumed $\varphi = h, hu, hv$. Here and analogously to the 1D formulation (3.9), we simply set

$$\begin{aligned}
\varphi^{n+1}_{i,j} = (L\varphi)^{n+1-}_{i,j} &- \frac{\Delta t}{\Delta x}\left(u^*_{i+\frac{1}{2},j}(L\varphi)^{n+1-}_{i+\frac{1}{2},j} - u^*_{i-\frac{1}{2},j}(L\varphi)^{n+1-}_{i-\frac{1}{2},j}\right) +\\
&- \frac{\Delta t}{\Delta y}\left(v^*_{i,j+\frac{1}{2}}(L\varphi)^{n+1-}_{i,j+\frac{1}{2}} - v^*_{i,j-\frac{1}{2}}(L\varphi)^{n+1-}_{i,j-\frac{1}{2}}\right),
\end{aligned} \tag{4.7}$$

where

$$(L\varphi)^{n+1-}_{i-\frac{1}{2},j} = \begin{cases} (L\varphi)^{n+1-}_{i-1,j} & \text{if} \quad u^*_{i-\frac{1}{2},j} > 0\\ (L\varphi)^{n+1-}_{i,j} & \text{if} \quad u^*_{i-\frac{1}{2},j} \le 0, \end{cases}$$

and

$$(L\varphi)^{n+1-}_{i,j-\frac{1}{2}} = \begin{cases} (L\varphi)^{n+1-}_{i,j-1} & \text{if} \quad v^*_{i,j-\frac{1}{2}} > 0\\ (L\varphi)^{n+1-}_{i,j} & \text{if} \quad v^*_{i,j-\frac{1}{2}} \le 0. \end{cases}$$

The Exner equation. As a natural extension of (3.11), we set

$$z_{i,j}^{n+1} = z_{i,j}^{n} - \zeta \frac{\Delta t}{\Delta x}\Big(u^*_{i+\frac{1}{2},j}\Big(\frac{q_{b,x}}{u}\Big)^{n+1-}_{i+\frac{1}{2},j} - u^*_{i-\frac{1}{2},j}\Big(\frac{q_{b,x}}{u}\Big)^{n+1-}_{i-\frac{1}{2},j}\Big) + \\ - \zeta \frac{\Delta t}{\Delta y}\Big(v^*_{i,j+\frac{1}{2}}\Big(\frac{q_{b,y}}{v}\Big)^{n+1-}_{i,j+\frac{1}{2}} - v^*_{i,j-\frac{1}{2}}\Big(\frac{q_{b,y}}{v}\Big)^{n+1-}_{i,j-\frac{1}{2}}\Big)$$

with

$$\big(\frac{q_{b,x}}{u}\big)^{n+1-}_{i+1/2,j} = \begin{cases} \big(\frac{q_{b,x}}{u}\big)\Big((L\mathbf{u})^{n+1-}_{i+1,j}\Big) & \text{if} \quad u^*_{i+1/2,j} \le 0 \\ \big(\frac{q_{b,x}}{u}\big)\Big((L\mathbf{u})^{n+1-}_{i,j}\Big) & \text{if} \quad u^*_{i+1/2,j} > 0, \end{cases}$$

and

$$\big(\frac{q_{b,y}}{v}\big)^{n+1-}_{i,j+1/2} = \begin{cases} \big(\frac{q_{b,y}}{v}\big)\Big((L\mathbf{u})^{n+1-}_{i,j+1}\Big) & \text{if} \quad v^*_{i,j+1/2} \le 0 \\ \big(\frac{q_{b,y}}{v}\big)\Big((L\mathbf{u})^{n+1-}_{i,j}\Big) & \text{if} \quad v^*_{i,j+1/2} > 0, \end{cases}$$

where a possible discretization of the evolution equations for Lu and Lv read

$$(Lu)^{n+1-}_{i,j} = (Lu)^{n}_{i,j} + \Delta t \frac{u_{i+1,j}+u_{i,j}}{2}\Big(\frac{1}{\Delta x}(u^*_{i+\frac{1}{2},j} - u^*_{i-\frac{1}{2},j}) + \\ + \frac{1}{\Delta y}(v^*_{i,j+\frac{1}{2}} - v^*_{i,j-\frac{1}{2}})\Big) - \Delta t \frac{\hat{s}_{i+\frac{1}{2},j} + \hat{s}_{i-\frac{1}{2},j}}{2}$$

and

$$(Lv)^{n+1-}_{i,j} = (Lv)^{n}_{i,j} + \Delta t \frac{v_{i,j+1}+v_{i,j}}{2}\Big(\frac{1}{\Delta x}(u^*_{i+\frac{1}{2},j} - u^*_{i-\frac{1}{2},j}) + \\ + \frac{1}{\Delta y}(v^*_{i,j+\frac{1}{2}} - v^*_{i,j-\frac{1}{2}})\Big) - \Delta t \frac{\hat{s}_{i,j+\frac{1}{2}} + \hat{s}_{i,j-\frac{1}{2}}}{2}$$

where $\hat{s}_{i+\frac{1}{2},j} = g((h+z)_{i+1,j} - (h+z)_{i,j})/\Delta x$ and $\hat{s}_{i,j+\frac{1}{2}} = g((h+z)_{i,j+1} - (h+z)_{i,j})/\Delta y$.

2D extension of the second-order scheme. We now briefly discuss the extension of the second-order scheme, distinguishing among the Exner equation and the Lagrangian and projection steps for the shallow water system. Once again we reach the second order of accuracy in time exploiting the Runge-Kutta procedure, which is applied to the Lagrangian and projection step together. As expected, the overall strategy is analogous to what we have done for the 1D case.

Regarding the Lagrangian step, we proceed as usual and compute the numerical fluxes $u^*_{i+\frac{1}{2},j}$, $v^*_{i,j+\frac{1}{2}}$, $\Pi^*_{i+\frac{1}{2},j}$ and $\Pi^*_{i,j+\frac{1}{2}}$, but also the speeds $a_{i+1/2,j}$ and $a_{i,j+1/2}$ using left and right interfaces values defined by means of reconstructed polynomials as in the 1D case, namely

$$\mathbf{V}^n_{i+1/2L,j} = \mathbf{V}^n_{i,j} + \Delta^{x,t}_{i,j}\frac{\Delta x}{2}, \quad \mathbf{V}^n_{i+1/2R,j} = \mathbf{V}^n_{i+1,j} - \Delta^{x,t}_{i+1,j}\frac{\Delta x}{2} \tag{4.8}$$

in the x direction, and

$$\mathbf{V}^n_{i,j+1/2L} = \mathbf{V}^n_{i,j} + \Delta^{y,t}_{i,j}\frac{\Delta y}{2}, \quad \mathbf{V}^n_{i,j+1/2R} = \mathbf{V}^n_{i,j+1} - \Delta^{y,t}_{i,j+1}\frac{\Delta y}{2} \tag{4.9}$$

along the y axis, where we have set $\mathbf{V}=(h,hu,hv)^T$. At this stage, we only need to define the slopes $\Delta_{i,j}^{x,t}$, $\Delta_{i,j}^{y,t}$ which are computed exactly as in the 1D case thanks to the definition of fluctuations in the x, respectively y, direction and considering that the $y=y_j$, resp. $x=x_i$, is fixed and using reconstructed stationary solutions direction by direction. The details are left to the reader. In particular, such a strategy guarantees the well-balanced property of the numerical scheme, since the slopes turn out to be null under the "lake at rest" conditions.

Regarding the transport step, we consider a direct 2D extension of (3.17) namely

$$\begin{aligned}
X_{i,j}^{n+1} = {} & (LX)_{i,j}^{n+1-} + \\
& - \frac{\Delta t}{\Delta x}\left(u^*_{i+\frac12,j}(LX)^{n+1-}_{i+\frac12,j}\left(\frac{\xi_{1,i+\frac12}+\hat\xi_{1,i+\frac12}}{2}\right) - u^*_{i-\frac12,j}(LX)^{n+1-}_{i-\frac12,j}\left(\frac{\xi_{1,i-\frac12}+\hat\xi_{1,i-\frac12}}{2}\right)\right) \\
& - \frac{\Delta t}{\Delta y}\left(v^*_{i,j+\frac12}(LX)^{n+1-}_{i,j+\frac12}\left(\frac{\xi_{2,j+\frac12}+\hat\xi_{2,j+\frac12}}{2}\right) - v^*_{i,j-\frac12}(LX)^{n+1-}_{i,j-\frac12}\left(\frac{\xi_{2,j-\frac12}+\hat\xi_{2,j-\frac12}}{2}\right)\right),
\end{aligned}$$

where we have used clear notations which are based on classical first-order polynomial reconstructions of the Lagrangian unknowns (LX) in each direction as in the 1D case, with $X=h,hu,hv$.

Finally, exploiting also the reconstructed values for Lu and Lv and using again classical notations, we suggest a direct 2D extension of (3.11) namely

$$\begin{aligned}
z_{i,j}^{n+1} = {} & z_{i,j}^n - \zeta\frac{\Delta t}{\Delta x}\left(u^*_{i+1/2,j}\left(\frac{q_{b,x}}{u}\right)^{n+1-}_{i+1/2,j} - u^*_{i-1/2,j}\left(\frac{q_{b,x}}{u}\right)^{n+1-}_{i-1/2,j}\right) + \\
& - \zeta\frac{\Delta t}{\Delta y}\left(v^*_{i,j+1/2,}\left(\frac{q_{b,y}}{v}\right)^{n+1-}_{i,j+1/2} - u^*_{i,j-1/2}\left(\frac{q_{b,y}}{v}\right)^{n+1-}_{i,j-1/2}\right)
\end{aligned}$$

with a natural definition for the numerical fluxes $\dfrac{q_{b,x}}{u}$ and $\dfrac{q_{b,y}}{v}$. Again, the details are left to the reader since there is no ambiguity.

To conclude this 2D section, let us mention that both the schemes described here preserve the "lake at rest" stationary solutions. The proof is analogous to the one seen in 1D.

5. Numerical results

This section is devoted to the presentation of the simulations and outputs of the numerical schemes we described so far. Regarding the 1D time step value, at each time t^n we compute two different time steps, one for the acoustic system and the other for the transport part, which respectively read

$$\Delta t \le \mathrm{CFL}_l \frac{\Delta x}{\max\limits_j\{\max(\tau_j^n,\tau_{j+1}^n)a_{j+\frac12}\}},$$

and

$$\Delta t \le \mathrm{CFL}_t \frac{\Delta x}{\max\limits_j\{u^+_{j-\frac12}-u^-_{j+\frac12}\}},$$

where CFL_l and CFL_t are respectively the CFL numbers for the Lagrangian and the transport systems, and

$$u^+_{j-\frac12}=\max(u^*_{j-\frac12},0) \quad \text{and} \quad u^-_{j+\frac12}=\min(u^*_{j+\frac12},0).$$

Then, the final time step is taken as the minimum between the two. If working in 2D, the acoustic time step is automatically extended, it is enough to consider both directions, while the transport time step reads

$$\Delta t \leq \mathrm{CFL}_t \min_{i,j}\left\{\left\{\frac{u^+_{i-\frac{1}{2},j}-u^-_{i+\frac{1}{2},j}}{\Delta x}+\frac{v^+_{i,j-\frac{1}{2}}-v^-_{i,j+\frac{1}{2}}}{\Delta y}\right\}^{-1}\right\}.$$

Finally, if not otherwise specified, we take $\zeta=1$, $q_b=A_g u^3$ with $A_g=0.005$ for the Exner equation, and transmissive boundary conditions. For the CFL number we use $\mathrm{CFL}_l=0.45$ and $\mathrm{CFL}_l=0.25$ for the first and second order schemes respectively, while $\mathrm{CFL}_t=1$. When the 1D reference solution is inserted, it is computed exploiting the second-order scheme with decoupled approximation (3.10) for the Exner equation. Then, $M=2000$ cells are used, where $\Delta x=\frac{L}{M}$ with L the length of the channel.

5.1. 1D Test of order of accuracy and computational cost. Here we test the order of accuracy of the numerical schemes described previously. Let us consider a channel of length $L=20m$, $A_g=0.3$, $m=3$. The initial condition is given by null velocity and

$$\begin{cases} z_{IC}=0.1-0.01e^{-(x-10)^2} \\ h_{IC}=2-0.1e^{-(x-10)^2}. \end{cases}$$

We refer to paper [12] for this test case. The reference solution is computed using $M=4096$ cells and second order decoupled method. In Tables 5.1-5.2 we list the error in norm $\mathbf{L}^1$ and the empirical order of accuracy (EOA) for the water height h, the discharge q and the topography z of both the weakly coupled and decoupled approaches. We can see that both schemes reach the second order of accuracy.

Method	Mesh M	Variable	err $\mathbf{L}^1$	$O(\mathbf{L}^1)$	Variable	err $\mathbf{L}^1$	$O(\mathbf{L}^1)$
Decoupled	64	h	0.0268	–	hu	0.1175	–
	128		0.0083	1.6953		0.0354	1.7320
	256		0.0027	1.6185		0.0115	1.6249
	512		0.0007	1.8756		0.0031	1.8782
	1024		0.0002	1.9781		0.0008	1.9818
Weakly coupled	64	h	0.0268	–	hu	0.1175	–
	128		0.0083	1.6955		0.0354	1.7320
	256		0.0027	1.6182		0.0115	1.6248
	512		0.0007	1.8755		0.0031	1.8781
	1024		0.0002	1.9782		0.0008	1.9818

Table 5.1: *Errors and empirical convergence rates for variables h and hu in norm $\mathbf{L}^1$. Mesh of size $M=(64,128,256,512,1024,2048)$, $CFL_l=0.25$. Second-order decoupled and weakly coupled numerical schemes.*

Then, we compare the presented numerical schemes against the well-known HLL and Lax-Wendroff (LW) methods (path-conservative version) for which we refer to [15]. In particular, we list their errors in norm $\mathbf{L}^1$ and the CPU time, where we underline that the CPU value is listed for information purposes only and without optimizing the MATLAB code. Here the objective is to show that for close error values, the computational cost is comparable. Thus, in Tables 5.3-5.4 we observe that this is indeed the case. Notice that we only used the LP weakly coupled method at first and second order of accuracy. Then, it is not surprising to see that the LW scheme converges more rapidly than our

Method	Mesh M	Variable	err $\mathbf{L}^1$	$O(\mathbf{L}^1)$
Decoupled	64	z	0.1792×10^{-3}	–
	128		0.0544×10^{-3}	1.7190
	256		0.0182×10^{-3}	1.5785
	512		0.0050×10^{-3}	1.8761
	1024		0.0012×10^{-3}	1.9932
Weakly coupled	64	z	0.1824×10^{-3}	–
	128		0.0550×10^{-3}	1.7296
	256		0.0183×10^{-3}	1.5890
	512		0.0050×10^{-3}	1.8734
	1024		0.0013×10^{-3}	1.9792

Table 5.2: *Errors and empirical convergence rates for variable z in norm $\mathbf{L}^1$. Mesh of size $M=(64,128,256,512,1024,2048)$, $CFL_l=0.25$. Second-order decoupled and weakly coupled numerical schemes.*

	Error $\mathbf{L}^1$ of h				Error $\mathbf{L}^1$ of hu			
Mesh	1st LP	2nd LP	HLL	LW	1st LP	2nd LP	HLL	LW
32	0.0526	0.0270	0.0503	0.0113	0.2165	0.1167	0.1782	0.0449
64	0.0313	0.0085	0.0281	0.0032	0.1311	0.0361	0.1004	0.0130
128	0.0171	0.0028	0.0148	0.0008	0.0721	0.0118	0.0535	0.0033
256	0.0090	0.0008	0.0076	0.0002	0.0380	0.0033	0.0273	0.0008
512	0.0046	0.0002	0.0038	0.0001	0.0195	0.0009	0.0139	0.0002

Table 5.3: *Errors in norm $\mathbf{L}^1$ of h and hu using first-order LP, second-order LP, HLL and LW methods. Mesh of size $M=(32,64,128,256,512)$.*

	Error $\mathbf{L}^1$ of z $\times10^3$				CPU			
Mesh	1st LP	2nd LP	HLL	LW	1st LP	2nd LP	HLL	LW
32	0.2870	0.1850	7.9	0.1370	0.0868	0.1665	0.0613	0.0606
64	0.1530	0.0560	4.9	0.0340	0.0572	0.0949	0.0694	0.0733
128	0.0850	0.0190	2.8	0.0080	0.2026	0.3013	0.2134	0.2413
256	0.0460	0.0050	1.5	0.0020	0.6906	0.9519	0.7281	0.8239
512	0.0240	0.0010	0.8	0.0010	2.5868	3.5400	3.1066	3.1523

Table 5.4: *Errors in norm $\mathbf{L}^1$ of z and computational cost using first-order LP, second-order LP, HLL and LW methods. Mesh of size $M=(32,64,128,256,512)$.*

second-order method as the Lagrange-projection formalism implies a splitting of the original mathematical model, leading to the presence of more diffusion. On the other hand, the HLL outputs are comparable with our first-order LP scheme when considering the h and hu variables, whereas the HLL approximation of z appears to be clearly worse.

5.2. 1D Riemann problem: dam break on movable bottom. For this Riemann problem we refer to [3]. The length of the channel is $L=10m$ and the dam is placed in the middle. The ending time is $t_{end}=1s$. The initial condition is given by null velocity, flat topography and water height $h_L=2m$ if $x<L/2$, $h_R=0.125m$ if $x>L/2$. In Figure 5.1 we show the numerical results given by the first-order weakly coupled scheme exploiting two different meshes, in particular $M=200$ and $M=2000$ cells. In the second case, we observe that the first-order solution converges towards the reference one, while for $M=200$ the solution is less accurate in the plateau zone when considering the topography z. Next, in Figure 5.2, we present the results for the

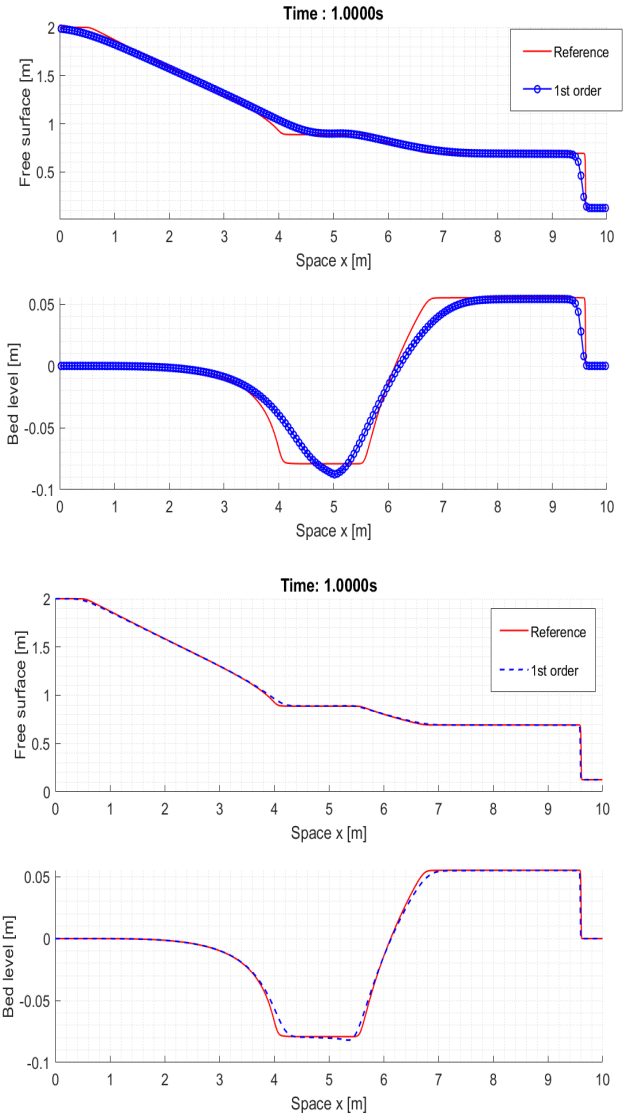

Fig. 5.1: *RP: dam break on movable bottom; free surface (up) and bed level (bottom). Reference solution (red) and first-order weakly coupled solution (blue). $M = 200$ cells (up) and $M = 2000$ cells (bottom).*

decoupled and weakly coupled second order numerical methods for different mesh sizes, $M = 100$, $M = 200$ and $M = 500$ cells. These two schemes give similar results and, in the topography outputs of both of them, we note some oscillations which decrease as we refine the mesh. We also observe that these oscillations are more accentuated in the decoupled scheme outputs.

5.3. 1D Riemann problems: comparing two formulations for q_b. The aim of this section is to compare two different formulations for q_b by considering two Riemann problems. In particular, we take into account the Grass formulation together

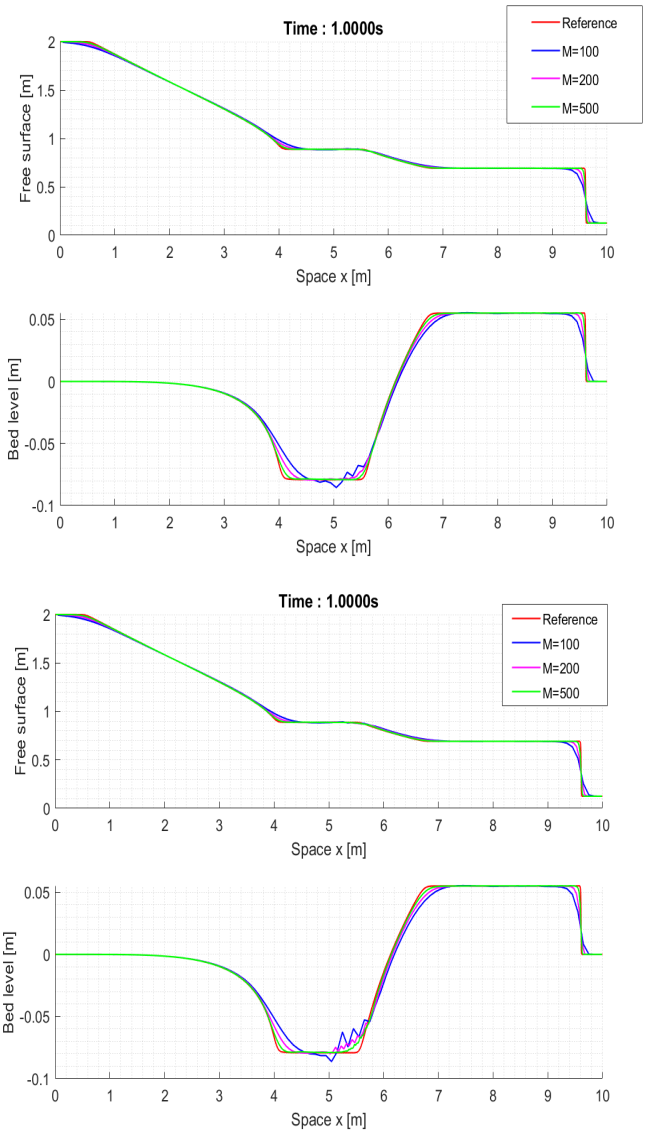

Fig. 5.2: *RP: dam break on movable bottom; free surface (up) and bed level (bottom). "Decoupled" (bottom) and "weakly coupled" (up) solutions. Mesh of size* $M=100$ *(blue line),* $M=200$ *(magenta line) and* $M=500$ *(green line) cells. Red line for reference solution.*

with the Meyer-Peter&Müller formula, which reads

$$q_b = 8Qsgn(u)(\theta-\theta_{cr})_+^{\frac{3}{2}} \quad \text{with} \quad Q = d\sqrt{gsd} \tag{5.1}$$

where d is the sediment diameter and s the relative density. Then, θ is the shear stress, for which we consider a Chezy-type approach, namely

$$\theta = \frac{1}{sgd}\frac{f_c u^2}{2},$$

for which refer to [10]. Observe that the main difference between the MPM formula and the Grass one is that q_b is not automatically different from zero when the velocity u is. Indeed, the shear critical value θ_{cr} has to be exceeded. If we take $\theta_{cr}=0$, it is clear that there exists a direct relation between formulas (1.4) and (5.1), that is to say

$$A_g = \frac{8}{sg}\left(\frac{f_c}{2}\right)^{\frac{3}{2}}.$$

In particular, here we take the following values, $\theta_{cr}=0.047$, $f_c=0.02$, $d=0.006$m and $s=1.666$ and, by consequence, $A_g=0.00049\ s^2/m$. Thus, the objective of this subsection is dual: On one hand we show that considering different formulations for q_b could lead to different results and, most important, that our numerical schemes can be applied even when considering other formulas for the solid transport discharge q_b. Indeed, nothing in particular has to be changed in the numerical strategy.

Let us consider a channel of length $L=50$m and gate in the middle. Here we take as initial conditions flat topography and zero velocity, together with $h_R=10^{-3}$m if $x<L/2$ and either $h_L=1$m or $h_L=0.2$m if $x\geq L/2$. Then, in Figure 5.3, we show the second-order weakly coupled solution computed with $M=1000$ cells at times $t_{End}=1$s, $t_{End}=3$s and $t_{End}=5$s. We can see that for $h_L=1$m there is a minimal difference between Grass and MPM formulas as the critical value θ_{cr} is almost immediately overcome. Conversely, we observe a greater difference in the bed elevation solution when considering $h_L=0.2m$. We refer again to [10] for similar analysis. Finally, we notice that some spurious oscillations appear in the second-order results also for these two Riemann problems.

5.4. 1D sub-critical and supercritical regions. For the following two numerical tests we refer to paper [21]. As initial condition we consider the sub-critical steady state

$$\begin{cases} hu(x,t=0)=0.5 \\ z(x,t=0)=0.1(1+e^{-(x-5)^2}) \\ \frac{u^2}{2}+g(h+z)=6.386, \end{cases}$$

while the length of the channel is $L=10.0m$. In Figure 5.4 we show the results of the first and second-order numerical schemes computed with $M=200$. We consider both $A_g=0.005$ (top) and $A_g=0.07$ (bottom). In both cases, the results are satisfying. In work [21], the authors noted that a splitting numerical scheme could produce oscillations in the solution of this numerical test, but reducing the CFL number could remedy the problem. By splitting numerical scheme, they mean a method which solves before the shallow water system for a fixed topography, and then updates the bed level according to the Exner equation. For our method it is not necessary to further decrease the CFL number due to the Lagrange-projection splitting whose numerical diffusion is sufficient as it comes from both steps. Then, in the same paper [21], the authors presented another test case in which the oscillations of the numerical solution of the splitting method could not be removed, even by reducing the CFL number. In Figure 5.5 we show that our solution does not present any oscillation. The decoupled method outputs are not reported as they are very close to the weakly coupled ones. For this last test case, the coefficient A_g is kept null until time $t=15s$ is reached, then the value $A_g=0.0005$

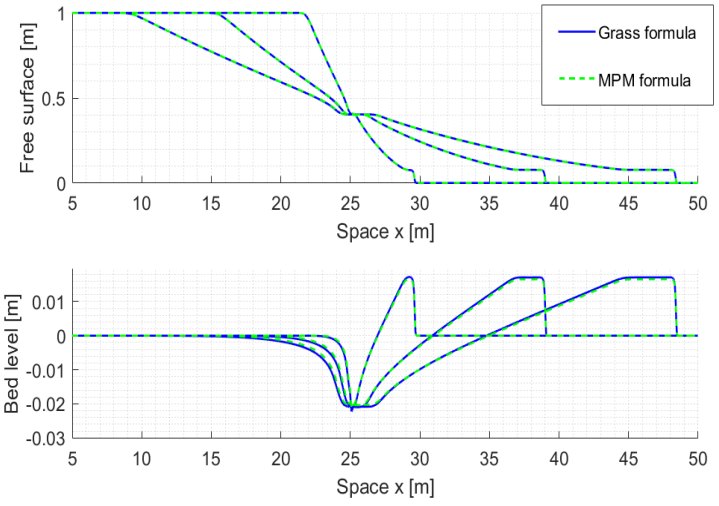

(a) $h_L = 1\text{m}$

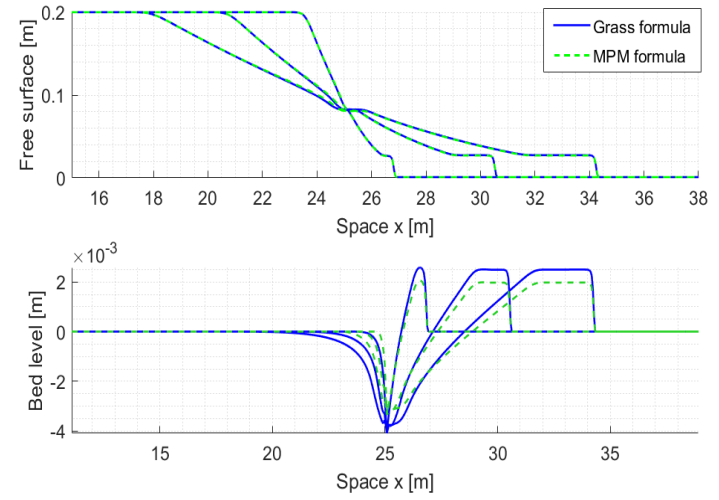

(b) $h_L = 0.2\text{m}$

Fig. 5.3: *RP: comparison between Grass (blue line) and MPM (green dashed line) formulas for q_b; free surface and bed level solution. Second-order "Weakly coupled" output at time $t_{End} = 1s$, $t_{End} = 3s$ and $t_{End} = 5s$, $M = 1000$ cells. Initial condition $h_L = 1m$ (up) and $h_L = 0.2m$ (bottom).*

is used. As initial condition we considered

$$\begin{cases} hu(x, t=0) = 0.6 \\ z(x, t=0) = 0.1(1 + e^{-(x-5)^2}) \\ h(x, t=0) + z(x, t=0) = 0.4. \end{cases}$$

Note that in this test case we have both sub-critical and supercritical regions.

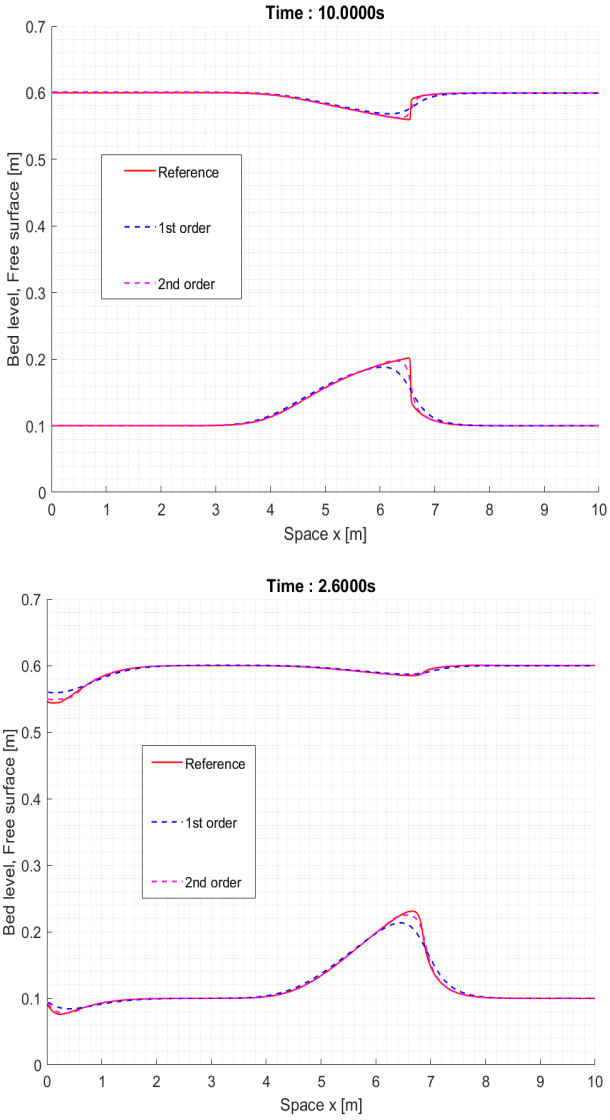

Fig. 5.4: *Flow over a movable bump; bed level z and free surface $z+h$; $A_g = 0.005$ (up) and $A_g = 0.07$ (bottom). First (blue) and second-order (magenta) weakly coupled solutions with $M = 200$ cells. Reference solution in red.*

5.5. 1D "lake at rest" solution and perturbation. This numerical test is useful to check the well-balanced property of the numerical scheme as we start considering a stationary solution and then we insert some perturbations. For the numerical tests of this section, see [19]. Thus, let us consider as initial condition null velocity, $h(x,t=0)+z(x,t=0)=3m$ and

$$z(x,t=0)=\begin{cases} 2+0.25(cos(10\pi(x-0.5))+1) & \text{if} \quad 1.4<x<1.6 \\ 2 & \text{otherwise.} \end{cases}$$

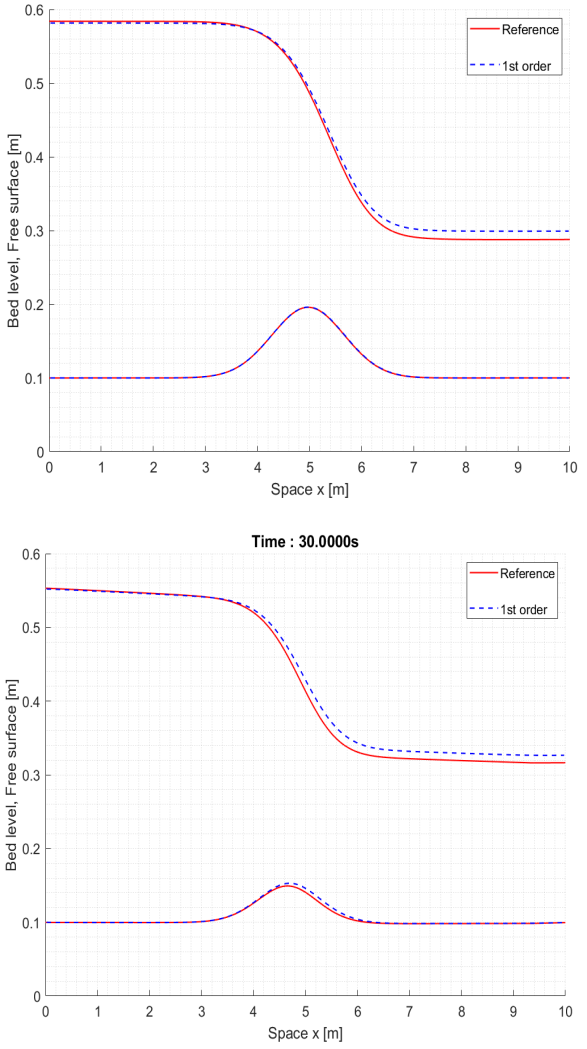

Fig. 5.5: *Free surface and bed level,* $M=200$ *cells,* $t_{end}=16.2s$ *(up) and* $t_{end}=30s$ *(bottom). Reference solution (red) and first-order weakly coupled solution (blue).*

The length of the channel is $L=2.0m$. Both first and second-order schemes maintain the steady state up to an error of order 10^{-15}.

As a second step, let us introduce small perturbations, namely we impose

$$h(x,t=0)=\begin{cases}3-z(x,t=0)+0.001 & \text{if} \quad 1.1<x<1.2\\ 3-z(x,t=0) & \text{otherwise.}\end{cases}$$

In Figure 5.6 we compare the results of first and second order numerical schemes against the reference solution. We observe that the outputs are satisfying and in agreement with the ones showed in work [19], no spurious oscillations appear. Clearly, the second order results are less diffusive than the first-order one.

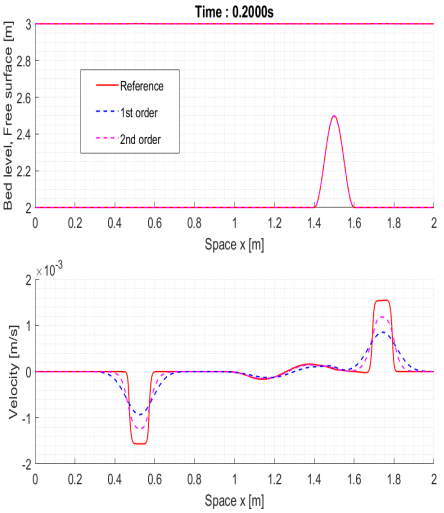

Fig. 5.6: *Propagation of perturbation; bed level z and free surface $z+h$ (top), velocity (bottom). First (blue) and second-order (magenta) weakly coupled solutions with $M=200$ cells. Reference solution in red.*

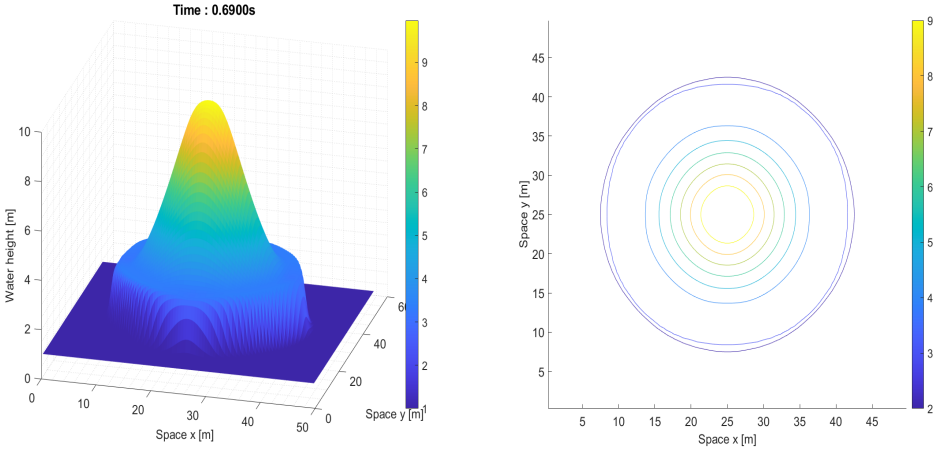

Fig. 5.7: *2D circular dam break on wet bed; water height (left) and its contour plot (right). 2D extension of first-order scheme solution. $M=100$ cells, $t_{End}=0.69s$ and $CFL_l=0.45$.*

5.6. Circular dam break on wet bed. Let us now consider test problems in 2 dimensions. In this first test, the Exner equation is not taken into account, refer to [41]. The domain is a $L\times L$ square with $L=50$m. Here as initial condition we consider a flat topography, null velocities in both the x and y directions and water height

$$h(x,y,t=0)=\begin{cases}10 & \text{if} \quad r\leq 11\text{m}\\ 1 & \text{if} \quad r>11\text{m},\end{cases}$$

with $r=\sqrt{(x-25)^2+(y-25)^2}$. Thus, we are considering a cylindrical dam that instantaneously breaks at the beginning time $t=0$s. The ending time $t_{\text{End}}=0.69$s. Satisfying results of the first order scheme are reported in Figure 5.7.

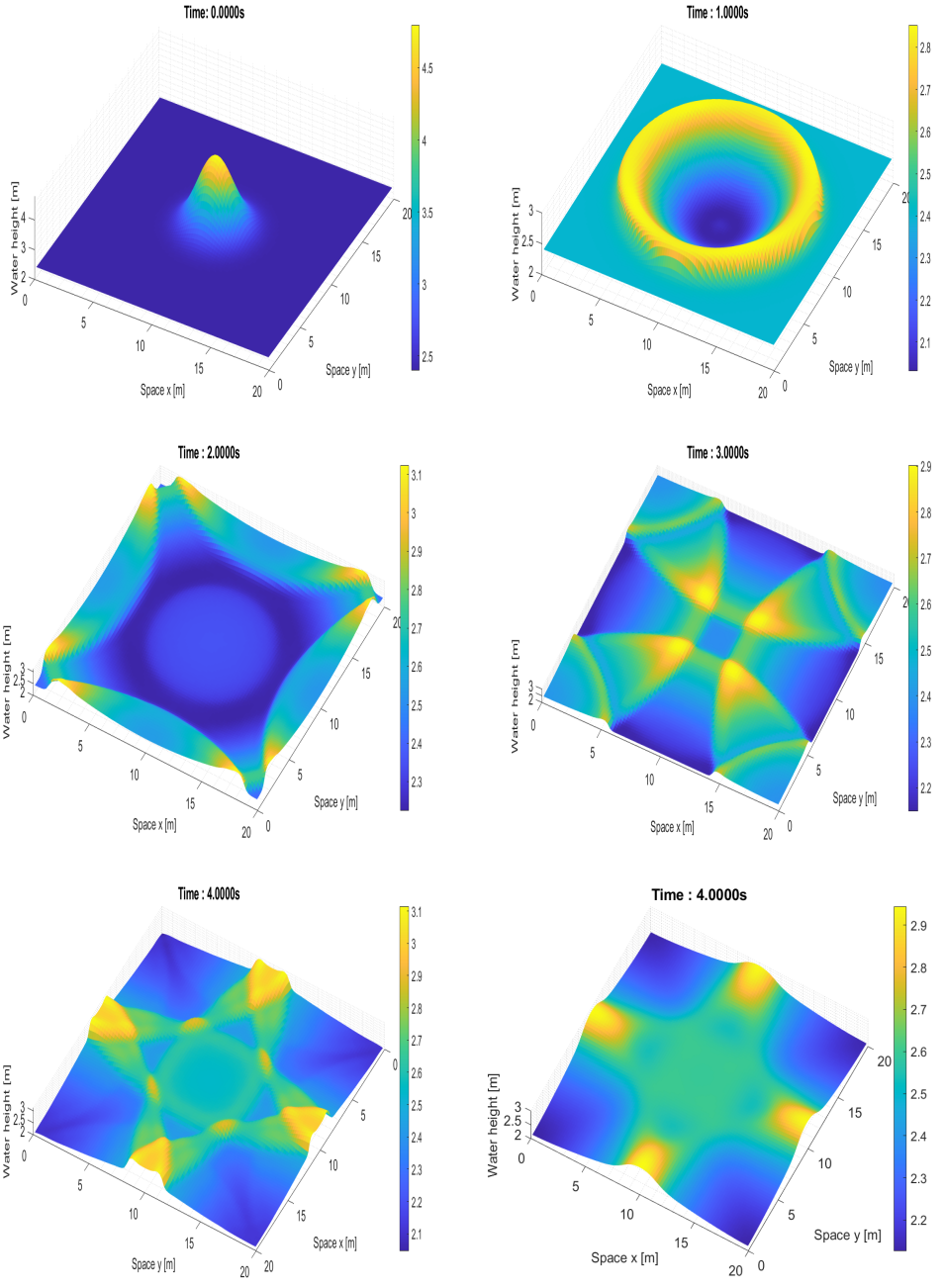

Fig. 5.8: *Water drop in a basin; water height at time* $t=0s$ *(up, left),* $t=1s$ *(up, right),* $t=2s$ *(middle, left),* $t=3s$ *(middle, right) and* $t=4s$ *(bottom).* $M=100$ *cells,* $CFL_l=0.25$ *and* $CFL_l=0.45$ *for the* $2D$ *extension of second and first order schemes, respectively.* $2D$*-extension of the* $1D$ *first-order scheme used only in the image on the bottom-right.*

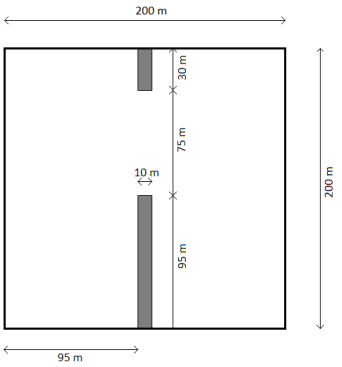

Fig. 5.9: *Geometry of the dam in the squared dam break test problem.*

5.7. Water drop in a basin. For this numerical test see [2]. Here we simulate a water drop in a basin and consequently reflective boundary conditions are used. A L-side square domain with $L=20$m is considered. The topography is still taken flat and constant in time. At initial time we assume $\mathbf{u}=(0,0)^t$ and

$$h(x,y,t=0)=2.4(1+e^{-0.25((x-10.05)^2+(y-10.05)^2)})$$

The outputs are shown in Figure 5.8 at time $t=1$s, $t=2$s, $t=3$s and $t=4$s respectively. The results agree with the ones reported in [2]. In particular, in the same Figure 5.8, we compare the results at time $t=4$s obtained using the 2D extensions of the first-order and second-order schemes. We can clearly see that the latter scheme gives less diffusive solutions under the same mesh $M=100$ cells.

5.8. 2D squared dam break. Once again we assume flat topography constant in time in a square domain of side $L=200$m. This time we consider a dam break problem with the dam position represented in Figure 5.9. We note a breach of length 75m which is instantaneously opened at time $t=0$. At initial time we also have null velocities and

$$h(x,y,t=0)=\begin{cases}10 & \text{if} \quad x\leq 100\text{m}\\ 5 & \text{if} \quad x>100\text{m}.\end{cases}$$

For more details about this test case, refer to [41]. The results for the water height and the velocity field are shown in Figure 5.10 and they appear to be in agreement with the reference outputs given in [41].

5.9. 2D flow over a smooth bump. The following test problem is useful to check the well-balanced property of the scheme, see [41]. The domain is a square of side $L=1$m and we consider the Grass formulation for the Exner equation with $A_g=1$ and $\zeta=1$. At initial time we assume null velocities,

$$z(x,y,t=0)=\max(0,0.25-5((x-0.5)^2+(y-0.5)^2)) \text{ and } h(x,y,t=0)=0.5-z(x,y).$$

Thus, the initial solution satisfies the "lake at rest" condition. Indeed, our 2D numerical schemes are able to preserve this kind of stationary solutions up to an error of order 10^{-15}.

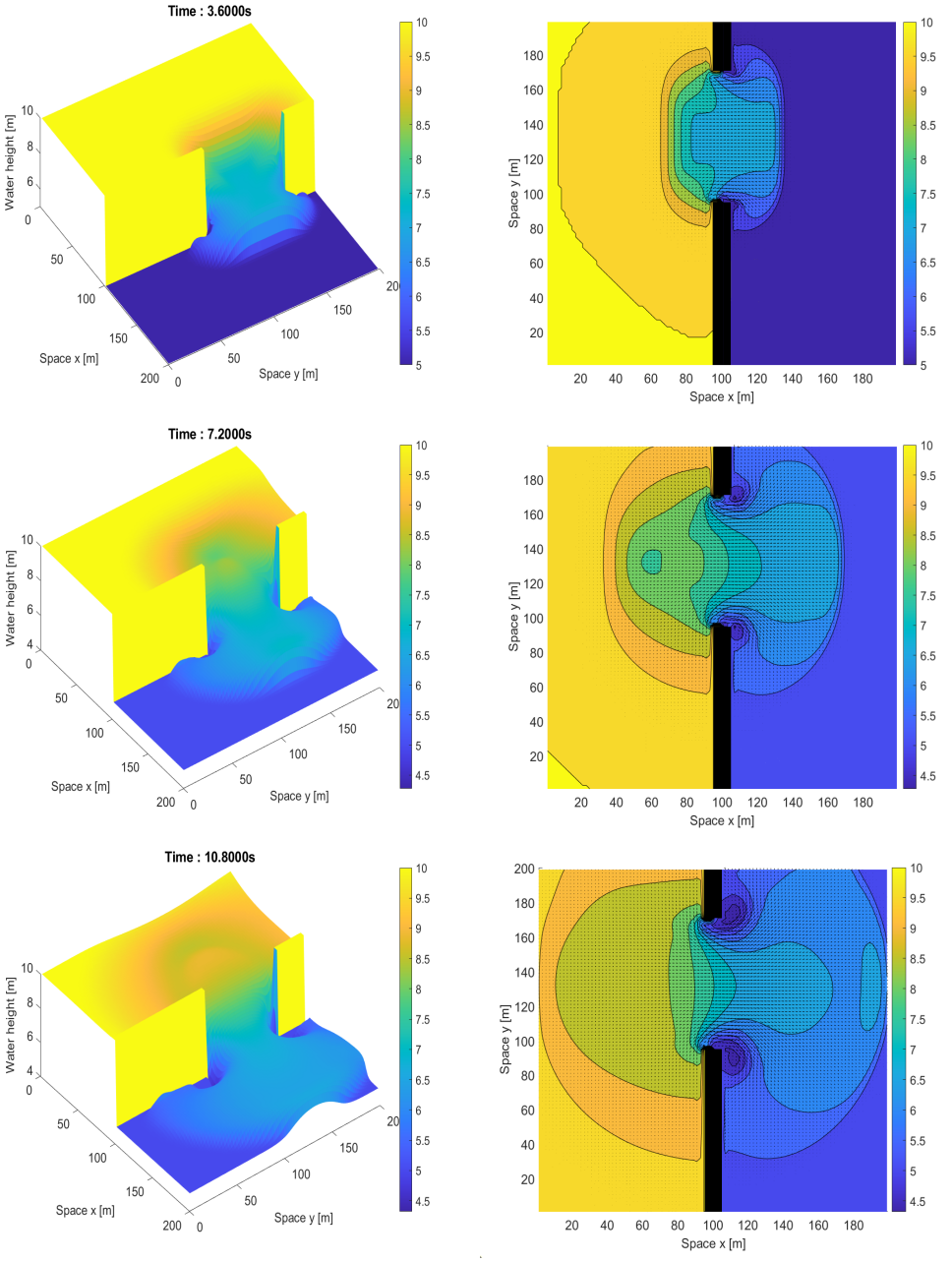

Fig. 5.10: *Squared dam break; water height (left) and contour plot and velocity field (right) at time* $t=3.6s$ *(up),* $t=7.2s$ *(middle) and* $t=10.8s$ *(bottom). Dam in black. 2D extension of second order scheme with* $M=100$ *cells and* $CFL_l=0.25$.

5.10. Conical dune of sand. This test case has been vastly used to validate numerical schemes for shallow water Exner system, here we do refer, for instance, to [4, 29]. When considering the Grass formulation for the sediment discharge, we take porosity $\rho_0=0.4$, where we recall that $\zeta=\frac{1}{1-\rho_0}$. The domain is a $L\times L$ square with

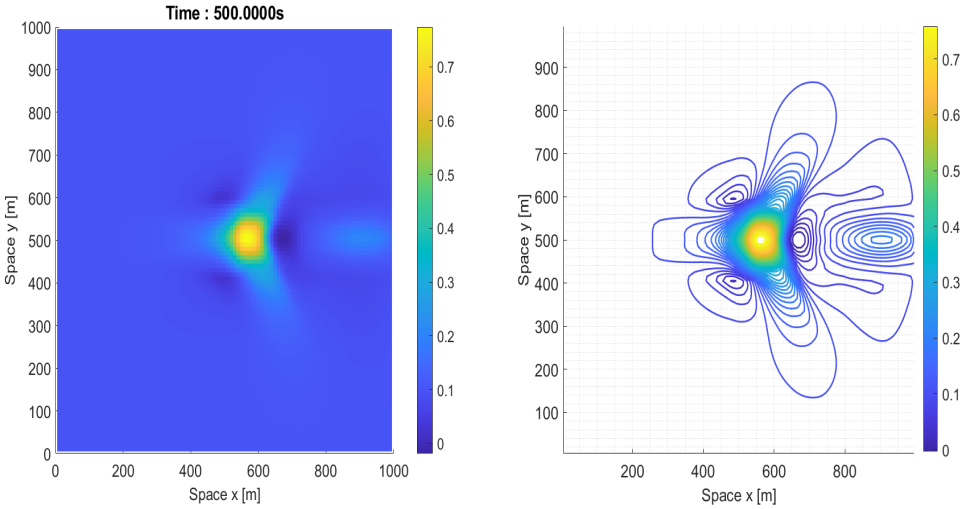

Fig. 5.11: *Conical dune of sand; fast interaction* $A_g = 1$. *Bed level (left) and contour plot (right) at time* $t = 500s$. *2D extension of second order scheme with* $M = 100$ *cells and* $CFL_l = 0.25$.

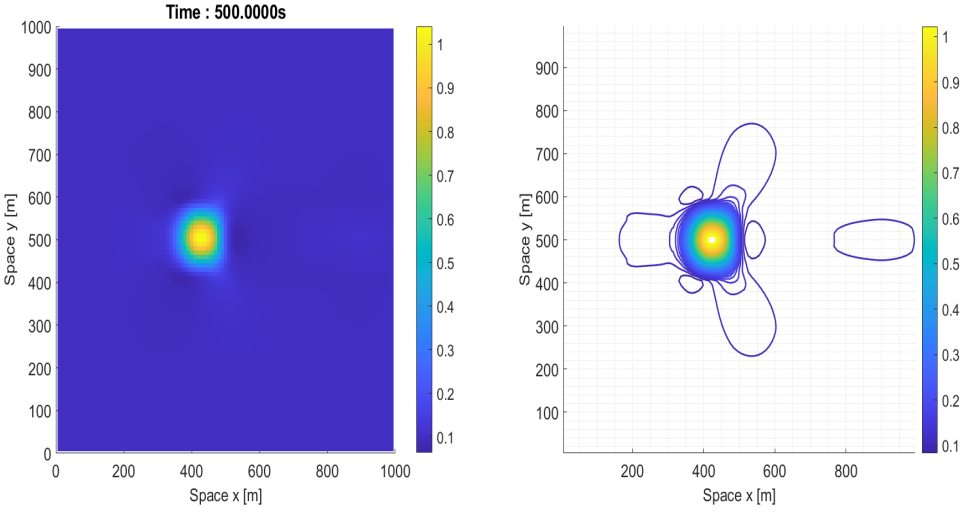

Fig. 5.12: *Conical dune of sand; medium interaction* $A_g = 0.1$. *Bed level (left) and contour plot (right) at time* $t = 500s$. *2D extension of second order scheme with* $M = 100$ *cells and* $CFL_l = 0.25$.

$L = 1000$m. At time $t = 0$, we impose

$$z(x,y,t=0) = \begin{cases} 0.1 + (\sin(\frac{\pi(x-300)}{200}))^2 (\sin(\frac{\pi(y-400)}{200}))^2 & \text{if} \quad 300 \le x \le 500,\ 400 \le y \le 600 \\ 0.1 & \text{otherwise,} \end{cases}$$

$$h(x,y,t=0) = 10 - z(x,y,t=0),$$

$$u(x,y,t=0) = \frac{10}{h(x,y,0)} \quad \text{and} \quad v(x,y,t=0) = 0.$$

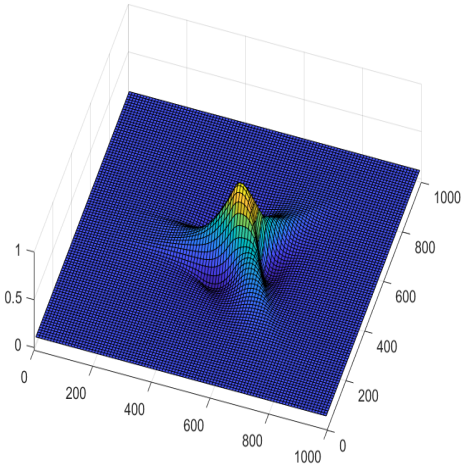

Fig. 5.13: *Conical dune of sand; slow interaction* $A_g = 0.001$. *Bed elevation computed with* $2D$ *extension of second order scheme with* $M = 100$ *cells and* $CFL_l = 0.25$.

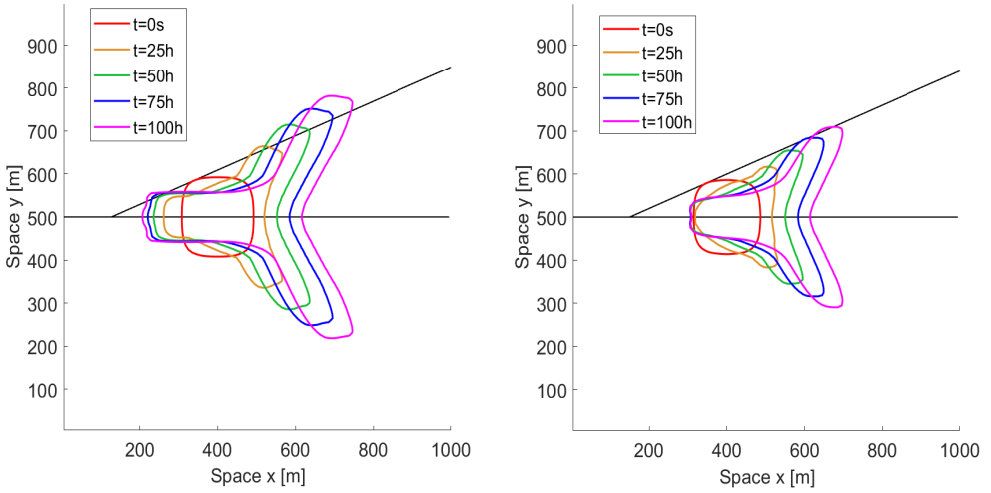

Fig. 5.14: *Conical dune of sand; slow interaction* $A_g = 0.001$. *Reference angle (black line) and iso-level at times* $t = 0s$ *(red),* $t = 25h$ *(orange),* $t = 50h$ *(green),* $t = 75h$ *(blue),* $t = 100h$ *(magenta). Iso-level* $z = 0.12$ *(left) and* $z = 0.15$ *(right).* $2D$ *extension of second order scheme with* $M = 100$ *cells and* $CFL_l = 0.25$.

Here, as boundary conditions, we assume that at the upstream we impose $u(x,y,t) = \frac{10}{h(x,y,t)}$ while the other boundaries are usual transmissive conditions.

Then, we start considering two different cases: in the first one we take $A_g = 1$ and ending time $t_{\text{End}} = 500$s, thus we are assuming a fast interaction between the flow and the sediments. As second case, we diminish the value of A_g, namely we impose $A_g = 0.1$, thus the strength of the interaction decreases. The outputs for these two test cases can be found in Figures 5.11 and 5.12, respectively. The results are in agreement with the ones reported in [4] even if more diffusive due to a coarser mesh size ($M = 100$ cells).

Finally, we consider a slow interaction case with $A_g = 0.001$. The aim of this simulation is to observe what is the spreading angle of the dune. Indeed, for slow water-sediment interaction cases, namely $A_g < 0.01$, the sediment bottom should expand according to a star-shaped pattern and an approximation of the spreading angle α has been proposed in the work of De Vriend [22]. In particular, considering the Grass formulation, the angle is given by

$$\tan(\alpha) = \frac{3\sqrt{3}(m-1)}{9m-1}$$

and thus, with $m = 3$, we should obtain $\alpha = 21.786789°$. Afterward, in Figure 5.13 we show the bed elevation at final time $t = 100$h, while in Figure 5.14 its contour plot is shown at different times. In particular, we consider the iso-levels $z = 0.12$ (left) and $z = 0.15$ (right) at times $t = 0$s, $t = 25$h, $t = 50$h, $t = 75$h, $t = 100$h. We also insert the analytical approximation of the spreading angle α in order to show that our second-order method is capable to compute the solution with enough accuracy. Indeed, for the iso-level $z = 0.12$, our results are comparable with the ones shown, for instance, in [20,29] as the majority of the spread of the dune is inside the cone. Then, since on the right we use a greater value for the iso-level, namely $z = 0.15$, it is not surprising to see that now almost all the spread is contained in the theoretical cone. See again the following works [4, 13, 20, 29] for similar considerations.

6. Concluding remarks

In this work a second-order well-balanced Lagrange-projection scheme for the shallow water Exner system has been presented in 1D. Its 2D extension has been proposed as well. In addition, both Grass and Meyer-Peter&Müller formulas for the solid transport discharge have been used. Numerical results proved the validity of the scheme. Usually, no unphysical oscillations are present in the first-order numerical outputs, while some could be found in the second-order extension. Moreover, in this work the Exner equation has been considered only in the transport step. Other strategies to take into account the Exner equation in the Lagrange-projection formalism are being explored and will be shortly submitted. Finally, it has already been observed that it could be interesting to develop the implicit approximation for the acoustic step in order to obtain faster numerical schemes, especially in subsonic regimes.

Acknowledgments. This work was partially supported by a grant from Région Île-de-France.

REFERENCES

[1] E. Audusse, F. Bouchut, M.O. Bristeau, R. Klein, and B. Perthame, *A fast and stable well-balanced scheme with hydrostatic reconstruction for shallow water flows*, SIAM J. Sci. Comput., 25:2050–2065, 2004. 1, 1

[2] E. Audusse and M.O. Bristeau, *A well-balanced positivity preserving "second-order" scheme for shallow water flows on unstructured meshes*, [Research Report] RR-5260, INRIA, 311–333, 2004. 5.7

[3] E. Audusse, C. Berthon, C. Chalons, O. Delestre, N. Goutal, M. Jodeau, J. Sainte-Marie, J. Giesselmann, and G. Sadaka, *Sediment transport modelling: Relaxation schemes for Saint-Venant-Exner and three layer models*, ESAIM Proc., 38:78–98, 2012. 1, 5.2

[4] E. Audusse, O. Delestre, L. Minh-Hoang, M. Masson-Fauchier, P. Navaro, and R. Serra, *Parallelization of a relaxation scheme modelling the bedload transport of sediments in shallow water flow*, ESAIM Proc. 43:80–94, 2013. 2, 5.10

[5] E. Audusse, C. Chalons, and P. Ung, *A simple three-wave approximate Riemann solver for the Saint-Venant-Exner equations*, Int. J. Numer. Meth. Fluids, 87:508–528, 2018. 1, 1, 2

[6] C. Berthon, S. Cordier, M. Le, and O. Delestre, *An analytical solution of shallow water system coupled to Exner equation*, C. R. Math., 350(3-4):183–186, 2012. 1

[7] C. Berthon and F. Foucher, *Efficient well-balanced hydrostatic upwind schemes for shallow-water equations*, J. Comput. Phys., 231:4993–5015, 2012. 1, 1

[8] M. Billaud Friess, B. Boutin, F. Caetano, G. Faccanoni, S. Kokh, F. Lagoutière, and L. Navoret, *A second order anti-diffusive Lagrange-remap scheme for two-component flows*, ESAIM Proc., 32:149–162, 2011. 1

[9] F. Bouchut, C. Chalons, and S. Guisset, *An entropy satisfying two-speed relaxation system for the barotropic Euler equations. Application to the numerical approximation of low Mach number flows*, Numer. Math., 145:35–76, 2020. 1

[10] R. Briganti, N. Dodd, D. Kelly, and D. Pokrajac, *An efficient and flexible solver for the simulation of the morphodynamics of fast evolving flows on coarse sediment beaches*, Int. J. Numer. Meth. Fluids, 69:859–877, 2012. 1, 2, 5.3

[11] R. Bürger, C. Chalons, and L. Villada, *Antidiffusive and random-sampling Lagrangian-remap schemes for the multiclass Lighthill-Whitham-Richards traffic model*, SIAM J. Sci. Comput., 35(6):1341–1368, 2013. 1

[12] M.J. Castro Díaz, E.D. Fernández-Nieto, and A.M. Ferreiro, *Sediment transport models in shallow water equations and numerical approach by high order finite volume methods*, Comput. Fluids, 37(3):299–316, 2008. 1, 1, 2, 5.1

[13] M.J. Castro Díaz, E.D. Fernández-Nieto, A.M. Ferreiro, and C. Parés, *Two-dimensional sediment transport models in shallow water equations. A second order finite volume approach on unstructured meshes*, Comput. Meth. Appl. Mech. Eng., 198:2520–2538, 2009. 2, 5.10

[14] M.J. Castro Díaz, C. Chalons, and T. Morales De Luna, *A fully well-balanced Lagrange-projection type scheme for the shallow-water equations*, SIAM J. Numer. Anal., 56(5):3071–3098, 2018. 1, 1, 1, 2, 2

[15] M.J. Castro, T. Morales de Luna, and C. Parés, *Well-balanced schemes and path-conservative numerical methods*, in R. Abgrall and C.-W. Shu (eds.), Handbook of Numerical Analysis, 18:131–175, 2017. 5.1

[16] C. Chalons, S. Kokh, and M. Girardin. *Large time step and asymptotic preserving numerical schemes for the gas dynamics equations with source terms*, SIAM J. Sci. Comput., 35(6):A2874–A2902, 2013. 2

[17] C. Chalons, M. Girardin, and S. Kokh, *An all-regime Lagrange-projection like scheme for the gas dynamics equations on unstructured meshes*, Commun. Comput. Phys., 20(1):188–233, 2016. 1, 2

[18] C. Chalons, M. Girardin, and S. Kokh, *An all-regime Lagrange-projection like scheme for 2D homogeneous models for two-phase flows on unstructured meshes*, J. Comput. Phys., 335:885–904, 2017. 1, 2

[19] C. Chalons, P. Kestener, S. Kokh, and M. Stauffert, *A large time-step and well-balanced Lagrange-projection type scheme for the shallow-water equations*, Commun. Math. Sci., 15(3):765–788, 2017. 1, 1, 2, 2, 2.1, 2.1, 5.5

[20] A. Chertock, A. Kurganov, and T. Wu, *Operator splitting based central-upwind schemes for shallow water equations with moving bottom topography*, Commun. Math. Sci., 18:2149–2168, 2020. 2, 5.10

[21] S. Cordier, M. Le, and T. Morales de Luna, *Bedload transport in shallow water models: why splitting (may) fail, how hyperbolicity (can) help*, Adv. Water Resour. 34(8):980–989, 2011. 2, 5.4

[22] H.J. De Vriend, *2DH mathematical modelling of morphological evolutions in shallow water*, Coast. Eng., 11:1–27, 1987. 5.10

[23] A. Del Grosso and C. Chalons, *Second-order well balanced Lagrange-projection schemes for blood flow equations*, Calcolo, 58, 2021. 1

[24] F. Duboc, C. Enaux, S. Jaouen, H. Jourdren, and M. Wolff, *High-order dimensionally split Lagrange-remap schemes for compressible hydrodynamics*, C. R. Math., 348(1-2):105–110, 2010. 1

[25] G. Gallice, *Solveurs simples positifs et entropiques pour les systémes hyperboliques avec terme source*, C.R. Math. Acad. Sci. Paris, 334:713–716, 2002. 2.1

[26] G. Gallice, *Positive and entropy stable Godunov-type schemes for gas dynamics and MHD equations in Lagrangian or Eulerian coordinates*, Numer. Math., 94:673–713, 2003. 2.1

[27] S. Gottlieb and C.W. Shu, *Total variation diminishing Runge-Kutta schemes*, Math. Comput., 67:73–85, 1998. 3.2

[28] A. Harten, P.D. Lax, and B. Van Leer, *On upstream differencing and Godunov-type schemes for hyperbolic conservation laws*, SIAM Rev., 25:35–61, 1983. 2.1

[29] J. Hudson, *Numerical techniques for morphodynamic modelling*, PhD thesis, University of Read-

ing, 2001. 2, 5.10
[30] C. Juez, J. Murillo, and P. García-Navarro, *A 2D weakly-coupled and efficient numerical model for transient shallow flow and movable bed*, Adv. Water Resour., 71:93–109, 2014. 2
[31] X. Liu, A. Mohammadian, A. Kurganov, and J.A. Infante Sedano, *Well-balanced central-upwind scheme for a fully coupled shallow water system modeling flows over erodible bed*, J. Comput. Phys., 300:202–218, 2015. 1
[32] R. Loubère, *Une méthode particulaire Lagrangienne de type Galerkin discontinu. Application à la mécanique des fluides et l'interaction laser/plasma*, These doctorale, Université Bordeaux, 2002. 1, 4
[33] P.H. Maire, R. Abgrall, J. Breil, and J. Ovadia, *A cell-centered Lagrangian scheme for two-dimensional compressible flow problems*, SIAM J. Sci. Comput., 29(4):1781–1824, 2007. 1, 4
[34] S. Martínez-Aranda, J. Murillo, and P. García-Navarro, *Comparison of new efficient 2D models for the simulation of bedload transport using the augmented Roe approach*, Adv. Water Resour., 153:103931,2021. 2
[35] R. Meurice and S. Soares-Frazão, *A 2D HLL-based weakly coupled model for transient flows on mobile beds*, J. Hydroinformatics, 22:1351–1369, 2020. 2
[36] V. Michel-Dansac, C. Berthon, S. Clain, and F. Foucher, *A well-balanced scheme for the shallow-water equations with topography*, Comput. Math. Appl., 72(3):568–593, 2016. 1
[37] V. Michel-Dansac, C. Berthon, S. Clain, and F. Foucher, *A well-balanced scheme for the shallow-water equations with topography or Manning friction*, J. Comput. Phys., 335:115–154, 2017. 1
[38] T. Morales de Luna, M.J. Castro Díaz, C. Parés Madroñal, and E.D. Fernández-Nieto, *On a shallow water model for the simulation of turbidity currents*, Commun. Comput. Phys., 6(2):848–882, 2009. 1
[39] T. Morales De Luna, M.J. Castro Díaz, and C. Chalons, *High order fully well-balanced Lagrange-projection scheme for shallow-water*, Commun. Math. Sci., 18(3):781–807, 2020. 1, 1, 2, 3.2, 3.2.1
[40] J. Murillo and P. García-Navarro, *An Exner-based coupled model for two-dimensional transient flow over erodible bed*, J. Comput. Phys., 229(23):8704–8732, 2010. 1, 2
[41] M. Seaïd, *Non-oscillatory relaxation methods for the shallow-water equations in one and two space dimensions*, Int. J. Numer. Meth. Fluids, 46(5):457–484, 2004. 5.6, 5.8, 5.9
[42] E.F. Toro and A. Siviglia, *PRICE: Primitive centred schemes for hyperbolic systems*, Int. J. Numer. Meth. Fluids, 42:1263–1291, 2003. 3.2.1
[43] E.F. Toro, *Riemann Solvers and Numerical Methods for Fluid Dynamics*, Third Edition, Springer-Verlag, 2009. 3.2.1
[44] C. Vreugdenhil, *Numerical Methods for Shallow Water Flow*, Water Science and Technology Library, Springer, 1:48, 1990. 1